DROSOPHILA AS A VERSATILE *IN VIVO* TESTBED FOR NANOMATERIAL TOXICITY ASSESSMENT

By
Sascha M. Vega-Alvarez

A thesis submitted in partial fulfillment of the requirements for the degree of:

MASTER OF SCIENCE
in
BIOLOGY

UNIVERSITY OF PUERTO RICO
MAYAGÜEZ CAMPUS
2012

Approved by:

Carlos Rinaldi, PhD Member, Graduate Committee	Date
Anthony V. Washington, PhD Member, Graduate Committee	Date
Franklin Carrero-Martínez, PhD President, Graduate Committee	Date
Elvia Camayd, PhD Representative of Graduate Studies	Date
Nanette Diffoot Carlo, PhD Chairperson of the Department	Date

ABSTRACT

Dramatic advances in nanomaterials synthesis and characterization provide promising possibilities for biomedical applications. Consequently, there is a growing demand for well-characterized, low cost toxicity assays for the validation of nanomaterials. Hence, we propose the use of the fruit fly, *Drosophila*, as a cost-effective model organism for the validation of novel nanomaterials. We conducted a product-specific science-based nanomaterial assessment using nanomaterial for biomedical applications at concentrations with practical relevance and at predicted environmental concentrations (PEC). We tested 8 nanomaterials at different concentrations: single-wall carbon nanotubes (SWCNT) and multi-wall carbon nanotubes (MWCNT); silver, gold, and titanium dioxide nanoparticles; and iron oxide (IO) nanoparticles (a) synthesized by co-precipitation coated with aminopropylsilane (APS) (Cop-IO-APS-Alexa-Biotin), (b) synthesized by co-precipitation coated with APS and carboxymethyldextran (CMDx) (Cop-IO-APS-CMDx), and (c) synthesized by thermo-decomposition coated with CMDx (Thermo-IO-CMDx). Our assessment allows us to test two different interaction routes; (1) direct microtransfer of nanomaterials into target tissues, and (2) direct contact-exposure in the developing embryo. The direct micro transfer route is based on simple developmental morphological milestones in *Drosophila* allowing for overall mortality quantification and identification of specific stage of mortality. The smallest concentrations were calculated based on PEC in water. In every case except for MWCNT these initial treatments presented no statistically relevant increase in toxic effect when compared to the control. The direct contact-exposure route serves as an assessment of nanomaterial transport across biological membranes. The results yielded are expected to lead to improvements in the design of nanostructures, the establishment of standardized regulations for characterization, handling and disposal of nanomaterials, and maximum allowable concentrations (MAC) in the environment. Furthermore, our cost-effective assessment has possibility of being conducted as a high-throughput screening methodology of nanomaterials amenable at every stage of R & D, and could be further developed to establish more specific molecular interactions.

RESUMEN

Importantes avances en la síntesis y caracterización de nanomateriales ofrecen posibilidades prometedoras para aplicaciones biomédicas. Debido a esto, existe una alta demanda de ensayos de toxicidad costo efectivos y bien caracterizados para la validación de nanomateriales. En respuesta a esta necesidad, proponemos la utilización de la mosca frutera, *Drosophila* como organismo modelo costoefectivo para la evaluación de nuevos nanomateriales. Evaluamos nanomaterials con posibles applicaciones biomédicas a concentraciones con relevancia práctica y concentraciones ambientales previstas. Probamos 8 nanomateriales en diferentes concentraciones: "single-wall carbon nanotubes" (SWCNT), "multi-wall carbon nanotubes" (MWCNT), nanopartículas de plata, oro y dióxido de titanio. Además de nanopartículas de magnetita (IO) (a) sintetizadas por coprecipitación y recubiertas con aminopropilsilano (APS) (Cop-IO-APS-Alexa-Biotin), (b) sintetizadas por coprecipitación y recubiertas con APS y carboximetildextrán (CMDX) (Cop-IO-APS-CMDx) y (c) sintetizado por descomposición térmica recubiertas con CMDx (Termo-IO-CMDX). Nuestro método nos permite probar dos posibles rutas de interacción; (1) microtransferencia en tegidos específicos y (2) exposición por contacto directo. La interacción por microtransferencia nos permite quantificar la mortalidad e identificar lase tapas especificas del desarrollo en donde ocurre la mortalidad. Las concentraciones más pequeñas fueron calculadas a base de PEC en agua. En todos los casos excepto para MWCNT, los tratamientos iniciales no presentan aumento estadísticamente relevante en efecto de toxicidad cuando se les comparan con el control. La interacción por contacto directo permite el análisis de transporte de nanomateriales a través de membranas biológicas. Se espera que estos hallazgos lleven a mejoras en el diseño de nanomateriales, el establecimiento de regulaciones sobre la caracterización, el manejo y desecho de nanomateriales, además de el establecimiento de concentración máxima permitida en el medio ambiente. Este trabajo presenta una experimentación costo efectiva con la posibilidad de llevarse a cabo como una metodología "high-throughput" para validación de nanomateriales, que puede utilizarse en todas las etapas del diseño y desarrollo de nanomateriales. Además que podría ser desarrollada aún más para establecer las interacciones moleculares envueltas.

DEDICATORIA

Esta tesis se la dedico a mi mamá, Ana M. Alvarez. Por ti soy quien soy y por todos tus sacrificios he llegado hasta aquí. Mis logros son tan míos como tuyos.

ACKNOWLEGMENTS

In my graduate studies at the University of Puerto Rico at Mayagüez a lot of people have contributed directly and indirectly to the fulfillment of my work. I wish to dedicate this section to recognize their support.

I want to start by thanking my advisor, Dr. Franklin Carrero-Martínez for giving me the opportunity to research under his guidance and supervision. I am really grateful to Carlos Marti, Rosa Martínez, Geidy Acevedo, Yue-Sai Jao and Whitney Stevens for their important assistance with embryo collection and preparation techniques. I want to thank our collaborator and thesis committee member from the Chemical Engineering Dept. Dr. Carlos Rinaldi for his guidance and support. From the Rinaldi Research Group I will also like to thank Alejandro López, Dr. Adriana Herrera, and Dr. Lenibel Santiago for synthesizing the employed nanomaterials and helping conduct ICP-MS analyses. The statistical analysis of the data was conducted with the help of Marisela Irizarry. Finally, I want to acknowledge the support and guidance of Dr. Vivian Navas who was always there unconditionally.

This work was supported by the United States Department of Defense (DoD) grant 55929LSH, the United States National Science Foundation (NSF) grants NSF-EPsCoR and NSF-IOS-0818243, and the National Institute of Health's (NIH) RISE-2-BEST Program grant NIH 1R25GM088023.

TABLE OF CONTENTS

LIST OF FIGURES……...……1

LIST OF TABLES…….....2

CHAPTER I: Introduction……...…….…….3

CHAPTER II: Literature Review…….……...…….…..8

Nanotoxicity……..……...……8

Drosophila melanogaster as a model organism……..……..…….10

Nanomaterials…….……...……13

CHAPTER III: Materials and Methods……..……...……..18

Pre-assay preparations……...18

Tissue-Specific Nanomaterial Assessment: Direct Microtransfer Interaction Route…….....……...21

Passive-Transport Nanomaterial Assessment: Direct Contact-Exposure Interaction Route……...…..……...25

CHAPTER IV: Figures.……...…….……...…..…..27

CHAPTER V: Results Tissue-Specific Nanomaterial Assessment…….……39

Introduction……..……..……...……39

Preliminary trials……..……...……...……39

Data Distribution Analysis……..……..……..……..….43

Non-Parametric Analysis…….……..……..……..……..……..…….43

Control trials……..……...……..…..……..……..…..……..44

Iron oxide…….……..……..……..…….....…..……...44

Silver, gold, titanium dioxide, single-wall carbon nanotubes, and multi-wall carbon nanotubes…….…….45

CHAPTER VI: Results: Passive Transport Nanomaterial Assessment.…….……48

Introduction…….....……..……48

Preliminary trials…….....……48

Inductively Coupled Plasma Mass Spectrometry Analysis.……...……....…….……48

CHAPTER VI: Tables and Graphs…….……..……..…..50
CHAPTER VII: Discussion……..……..…….66
CHAPTER VIII: Conclusions……..…….……..70
CHAPTER IX: References……...…….…..…….72

LIST OF FIGURES

Figure 1. *Drosophila* Life Cycle……..….27

Figure 2. Embryonic and Larval Development……..……..……..……28

Figure 3. Eggshell membranes……..…….29

Figure 4. Embryo mounting procedure…….....……30

Figure 5. Microscope, micromanipulator and microinjector setup……..……..31

Figure 6. Embryonic microtransfer procedure……..…….32

Figure 7. Post-injection Recovery……....……..……33

Figure 8. Microneedle visualization procedure…….…...…….……34

Figure 9. Laboratory-made microneedles……..……35

Figure 10. Microneedle Troubleshooting…….…….36

Figure 11. Morphology Prior and After Nanoparticle Interactions through Direct-Microtransfer…….……..……...…..……...…….……..37

Figure 12. Morphology Prior and After Nanoparticle Interactions through Direct Contact-exposure……..……..…….....…...…....……....……..38

LIST OF TABLES

Table 1. Microtransfered Volume Quantification…….……..50

Table 2. Average amount of nanoparticles per microtransfer.…….…….……..……...…50

Table 3. Statistical comparison of control groups through Fisher's exact test for unpaired samples.……...…..……...……...51

Table 4. Statistical comparison of H_2O vs IO-nanoparticle treatment through Fisher's exact test for unpaired samples.…..……..…….…….....51

Table 5. Statistical comparison of BSA 10% vs nanomaterial treatment through Fisher's exact test for unpaired samples.……..……...……..…...52

Table 6. ICP-MS Analysis of *Drosophila* embryos without nanomaterial treatment……...……...…….....……..……...……..…..53

Table 7. ICP-MS Analysis of materials involved in solutions or sample preparation……..……...……..…..……...……..…...……....53

Table 8. ICP-MS Analysis of *Drosophila* embryos subjected to IO-nanoparticle treatment.……...……..…….....…….....…….....54

Table 9. ICP-MS Analysis of *Drosophila* embryos subjected to silver, gold, and titanium dioxide nanoparticle treatment……...……...……..……55

CHAPTER I

INTRODUCTION

As the field of nanotechnology evolves novel biomedical applications for nanomaterials emerge and so does the concern for the hazardous effects they could have in both our health and environment. Consequently, there is a need for models that assess their implications and behavior within biological systems. **The purpose of this research is to present the fruit fly, *Drosophila melanogaster*, as a suitable *in vivo* model for nanomaterial assessment.**

Nanotechnology

According to *Drexle, 2004*, Richard Feynman's 1959 talk "There's Plenty of Room at the Bottom" is the first academic talk that dealt with the ideas and concepts of nanotechnology. Half a century has passed and today nanomaterials form part of a wide array of products ranging from biomedical employment to everyday-use. Today, nanotechnology is described as "the technology development at the atomic, molecular or macromolecular levels, in the length scale of approximately 1 - 100 nanometer range, to provide a fundamental understanding of phenomena and materials at the nanoscale and to create and use structures, devices and systems that have novel properties and functions because of their small and/or intermediate size" (NSTC/NSET, 2000).

Nanomaterials can be found in products such as paints, coatings, sunscreens, cosmetics, personal care products, stain-resistant clothing, food and food packaging, light-emitting diodes used in computers, cell phones, and digital cameras (Kimbrell, 2006). Nevertheless, they are also employed in more advance applications such as cellular therapy (cell labeling and targeting), cell sorting, tissue repair, drug delivery, magnetic resonance imagining (MRI), hyperthermia (heat treatment against cancerous cell) and magnetofection (transference of nucleic acids into a cell) (Gupta and Gupta, 2005; Dobson, 2008). Research and biomedical applications on cellular and molecular biology are endless.

The increase in nanomaterial production implies a higher risk of environmental as well as human exposure. (Mueller and Nowack, 2008). Is because of the extensive use of nanomaterials that researchers as well as agencies are putting a lot of efforts into understanding exposure risks

across a nanomaterial's life cycle (Kloepffer et al., 2007). Suggesting the consideration of exposure risks from manufacture to transport, use, and waste management for every specific nanomaterial. Although the research to be performed on nanomaterial life cycle assessments is seemingly endless we have taken a step forward by assessing the toxicological effects of a select group of nanomaterials employed in both daily use products and biomedical products from which traces have been found in the environment.

Nanotechnology: Lack of Regulations

Despite the widespread use of nanomaterials and possibilities of exposure, federal agencies such as *the* Environmental Protection Agency (EPA)[1], and the Federal Drug Administration (FDA)[2] have only recently started issuing regulations for their use. However, because of the lack of consensus on definitions only guidelines have been developed instead of a meaningful regulatory framework. The need for these regulations is clearly expressed in the memorandum for the heads of executive department and agencies of June 9, 2011 by the Office of Science and Technology Policy et al*.,* "Policy Principles for the U.S. Decision-Making Concerning Regulation and Oversight of Applications of Nanotechnology and Nanomaterials". In order to reach a consensus and establish clear and specific regulations for human and environmental safety we need to follow a science-based approach (Office of Science and Technology Policy et al*.,* 2011). Unfortunately, toxicity assessments have not been developed in tandem with this fast growing field mostly due to the ambiguity from one assessment to another. The ambiguity between assessments has been recently discussed in *Science*'s Policy Forum by *Hamburg, 2012* were this Commissioner for the FDA acknowledges the importance of a product-specific science-based approach for nanotoxicity assessment. By focusing on the development of product-specific assessments, conclusions will no longer be broad generalizations and will be in turn based on the specific properties of the nanomaterial: size, surface modifications, concentration, and exposure route. Our work presents a new product-specific science-based *in vivo* toxicity assessment.

---

[1] EPA Nano Guidance: EPA–HQ–OPP–2010-0197. http://www.gpo.gov/fdsys/pkg/FR-2011-06-17/pdf/2011-14943.pdf

[2] Draft- Guidance for Industry. Considering Whether an FDA-Regulated Product Involves the Application of Nanotechnology. FDA-2010-D-0530. http://www.fda.gov/RegulatoryInformation/Guidances/ucm257698.htm

Toxicity assessments: *in vivo* versus *in vitro*

Understanding the nanomaterial's behavior within a biological system gives us an idea of their ecological effects (Fischer and Chan, 2007). To understand nanomaterial hazards, the nanomaterial-cellular interactions have to be identified. Toxicity assessments can render the necessary evidence to establish the adverse effects a substance has in an organism at organ, tissue, and cellular levels. Therefore, nanotoxicity refers to the physical and chemical interactions of nanomaterials with a biological system that induce a toxic biological response.

When it comes to understanding the human body and how the systems, organs and specific cells work and interact with one another, the use of model organisms with analog mechanisms has proven to be a basic tool and in some cases the only. Model organisms, or *in vivo* models, have served as essential tools to understand and represent our complex reality by providing a simplified and accessible version (Chiba, 1999). In the last century, biological experimentation made a shift from *in vivo* assessment to *in vitro* because of new findings in terms of cellular organelles and genetics, and the need for single cell resolution (Vignais, Vignais, 2010). *In vitro* and *in vivo* assessments have been validated for different purposes and both present advantages as well as disadvantages.

In vitro assessments refer to the analysis of organs, tissues, cells, and biomolecules in an artificial environment, while *in vivo* take place in the context of an intact organism. *In vitro* studies provide valuable plataform for cell specific assessments such as: cell adhesion, internalization, intracellular processing and trafficking, cell signaling and nanomaterial-induced cell phenotype facilitating visualization (NNCO-NSET-NEHI, 2009). The primary advantage of *in vitro* assessments is their reductionist approach because it limits the scope of the research to study specific events of interest that would otherwise be more complicated in a complex functional organism.

In vivo assessments are performed using whole organisms in which spatial organization is almost unaltered and interactions are allowed to occur as normal as possible. *In vivo* assessments provide information in terms of: tissue toxicity, biodistribution, absorption, bioaccumulation, metabolism, excretion patterns, cell migration pattern disruption and the specific destabilization processes across the material's life cycle (Office of Science and Technology Policy et al., 2011).

Both *in vivo* and *in vitro* methods should aim to help in the establishment of an *in vitro-in vivo* extrapolation or correlation (Sutter, 1995). The complex processes within an organism can be broken down into specific mechanistic steps that can be studied separately *in vitro*. When these specific mechanisms have been described, *in vitro* assessments yields results that can be extrapolated to their *in vivo* counterpart.

***Drosophila* as an *in vivo* model**

According to the National Nanotechnology Initiative (NNI) Environmental, Health and Safety (EHS) research strategy, the efforts on nanotoxicity research should focus on development of cost effective, rapid assessment tools, and consensus-derived experimental protocols. Thus providing reproducible data, being versatile enough to be used in research and development, manufacturing, and use conditions that allow for multiple exposure contexts (NNCO-NSET-NEHI, 2009). In accordance to the previously mention, recently published letter by *Hamburg, 2012* on the importance of a product-specific science-based approach for nanotoxicity assessment. We propose the use of *Drosophila* as an *in vivo* model for the product-specific science-based assessment of nanomaterials, providing the advantages of both known *in vivo* and *in vitro* models.

Drosophila is one of the most important model organism because of its short and easy to manage life cycle (Fig. 1), completely sequenced and mapped genome, and the variety of genetic tools and molecular techniques available for it (Carrero-Martínez and Chiba, 2009). *Drosophila*'s single-cell resolution altogether with it's neuromuscular system consisting of a series of segmental repeats of well known pattern (Hoang and Chiba, 2001), allows for an accessible, simple and precise developmental staging not only from a morphological perspective but also from a molecular perspective. In addition, these single identifiable cells can be tracked throughout the entire embryonic development thanks to the clear cuticle during embryonic and larval stages. This in turn, allows us to study developmental effects of nanomaterials in a specific area or systems of interest as it occurs (Margaritis, et al*.,* 1980). Furthermore, *Drosophila* presents a cost effective alternative, because a female can lay as many as 3,000 eggs in her lifetime (Ashburner et al., 2004); providing a constant supply of individuals in every stage of development. Furthermore, due to its small size the amount of nanomaterial required for *in vivo*

testing is in the nanogram (ng) range compared to the micrograms used in rodents.

We have developed a cost-effective product-specific nanomaterial assessment with two different interaction routes. The first one, a direct microtransfer of nanomaterials into target tissues, which yield quantifiable mortality results based on simple developmental morphological milestones in *Drosophila*. Nanomaterials have shown promise as platforms for the successful delivery of bioactive compounds to diseased cells (Peer, et al. 2007). Our second exposure route, a direct contact-exposure in the developing embryo serves as an assessment of nanomaterial transport across biological membranes modeling environmental exposure, which could establish *Drosophila* as an important organism for establishing environmental nanomaterial pollution.

Our novel assessment was conducted using nanomaterial concentrations with practical relevance for both biomedical applications and predicted environmental concentrations, and allows for overall mortality quantification, identification of specific stage of mortality, and quantification of internalized nanomaterials. Furthermore, our assessment can be further developed to establish more specific molecular interactions. The results yielded are expected to lead to improvements in the design of nanostructures and the establishment of standardized regulations for characterization, handling, and disposal of nanomaterials.

CHAPTER II

LITERATURE REVIEW

Nanotoxicity

Nanotoxicity has emerged as a subfield of nanotechnology in response to a transition from academic to industrial applications (Fischer and Chan, 2007). Assessments in nanotoxicity can be performed both *in vitro* and *in vivo* each having their own advantages and disadvantages

In vitro toxicity assessment

Current *in vitro* cytotoxicity assessments include: cell viability, stress response and inflammatory response (Kroll et al., 2009; Lewinski et al*.,* 2008). These assessments are mostly conducted by colorimetric and fluorometric detections. *In vitro* cell viability is assessed by colorimetric determinations such as: mitochondrial activity (MTT); lactate dehydrogenase (LDH), which is used to evaluate necrotic activity; detection of intact lysosomes, by neutral red uptake; and fluorometric detection of caspase-3, which is an apoptosis marker. Stress response is assessed by fluorometric detection of reactive oxygen species, while inflammatory response is assessed by colorimetric detection of cytokine secretion through enzyme-linked immunosorbent assay (ELISA), which integrates antibodies and enzymatic detection reactions, for the quantification of inflammatory markers in cell culture (Kroll et al*.,* 2009). Even though these methods have been validated for the assessments of other chemical substances, multiple studies have presented data suggesting that nanoparticles may interfere with assay components or detection systems. For example, researchers have noticed that in colorimetric detection of MTT reduction metal ions can interfere with the reaction causing false negatives (Granchi et al*.,* 1996). On the downside, cells in culture do not always present their *in vivo* morphology, simulate a microenvironment's complexity, exposure route or dosing. Therefore, they are not able to replicate the mechanical and chemical signals between interacting cells and lack tissue and organ formation.

In vitro assessments have also proven to be cost effective and present the possibility of being high-throughput, providing rapid result acquisition, both characteristics that are missing in many *in vivo* models. Rogers et al., 2008 developed a high throughput *in vitro* assessment that

allowed for the quantification of oxidative stress exerted by nanomaterials in a biologically relevant matrix. Their assessment employs a Ferric reducing ability of serum (FRAS) assay that quantifies the antioxidant capacity of blood serum after being treated with nanomaterials. As with this example, high-throughput *in vitro* assessments tend to oversimplify a biological environment.

In vivo toxicity assessment

The most common *in vivo* nanotoxicity assessments use rats or mice as model organisms but other model organisms like *Caenorhabditis elegans, zebrafish* and *Drosophila* are gaining popularity (Pluskota, et al*.,* 2009; Mohan, et al*.,* 2010; Usenko et al*.,* 2007; Asharani et al., 2008; Fako and Furgeson, 2009; Liu, et al*.,* 2009). Rats and mice, being mammals, present an obvious advantage over other animal models for they are fairly similar to humans and can be used to study complicated processes underlying normal human development, diseases and behavior. Using rats or mice as model organisms allows scientists to mimic possible exposure routes that occur in humans, like inhalation (Sung et al., 2009), dermal exposure (Wu et al., 2009) and injections (Liu, et al., 2011). In addition, organ biodistribution and dose equivalencies like minimum lethal dose (MLD) and median lethal dose (LD50) can be directly extrapolated (Liu, et al., 2011**).** Rats have recently lost favor as animal models in some fields. The possibilities for genetic manipulation are reduced in this model because its genome does not tolerat**e** the insertion of foreign DNA to the extent of organisms like the mouse, *C. Elegans* or *Drosophila* (Hunter, 2008).

Another aspect to take into consideration when selecting a model organism for nanomaterial assessment is the amount of nanomaterials required for experimentation since this will be directly related to the organism's size. Taking this into account an adult rat (up to 25 cm) wouldn't be a cost effective model organism for it would need the largest amount of nanomaterials in comparison to mice (adult 7.5–10 cm), *zebrafish* (embryo 0.9-3.3 mm / adult 14 mm), *Drosophila* (embryo 0.5 mm / adult 3 mm) and *C. Elegans* (embryo 0.05 mm / adult 1 mm).

C. elegans and *Drosophila* possess many of the same advantages but differ mostly on the degree of tractability and accessibility that can be used in experimental manipulation. *Drosophila*

presents the possibility of assessing the six principle exposure routes: intravenous, dermal, subcutaneous, inhalation, intraperitoneal, and oral (Fischer and Chan, 2007). However, different exposure routes have not been fully assessed, because most researchers conduct trials through oral ingestion (Liu et al*.,* 2009; Ahamed et al*.,* 2010; Posgai et al*.,* 2011; Barandeh, et al*.,* 2012). However, oral ingestion is one of the harshest treatments a nanomaterial can undergo in a living organism when taking into account the extreme pH in the digestive system. Unless the experimentation is performed with a nanomaterial of inert core, the nanomaterial's surface coating can suffer from alterations thus resulting in toxic effects.

Oral ingestion is the most widely employed exposure route among nanotoxicity research in *Drosophila*. For example, *Liu* et al*., 2009* determined that larvae and adult flies exposed to carbon nanomaterials presented locomotor impairment and mortality. There is little comparison to expected environmental concentrations because this is an unlikely nanomaterial-oversaturated scenario. As a result, an indirect toxicity effect was interpreted as locomotor impairment, which can be misleading suggesting neurotoxic involvement instead of simple movement restriction caused by the fine particle coating deposited over the organism. The lack of practical relevance in terms of dosage and exposure routes is a common downfall in nanomaterial assessments (Liu, et al., 2009).

We have developed an alternative exposure method in *Drosophila* that allows comparisons against any nanomaterial concentration with practical relevance and can be further developed to establish more specific molecular interactions involved in toxicity reactions.

Drosophila melanogaster **as a model organism**

The use of *Drosophila* as a research organism dates to the beginning of the field of genetics in 1900's (Powell, 1997). The experimentation on this organism has expanded to other fields of biological science, building up a well-established knowledge base for more than a century. This ultimately resulted in its sequenced genome and the availability of mutants to simulate experimental conditions as well as human health conditions. *Drosophila* offers the possibility to perform *in vivo* studies in context of validated human disease models (Hirth, 2010; Gilbert, 2008; Chien et al*.,* 2002; Reiter et al*.,* 2001; Bernards and Hariharan, 2001), as a drug-screening model (Das and Cagan, 2010; Tickoo and Russell, 2002) and for understanding the

self-assembly process of the neuronal network (Carrero-Martínez and Chiba, 2009; Chiba, 1999). The wide array of research applications that use *Drosophila* further emphasize the value of this model organism for the rapid screening assessment of novel nanomaterials applications and toxicological implications (Liu, et al., 2009).

Life cycle

Drosophila's life cycle lasts between 9 to 10 days under ideal temperature (25°C) conditions (Fig. 1). Flies lay their embryos and ~24 hours after egg laying (AEL), embryos hatch into a first instar larva (L1). The L1 is a wandering stage in which the larvae feed on the surface of the medium. After ~ 48 hours AEL, it molts into a second instar (L2) and after ~72 hours AEL another molting occurs, resulting in the third instar larva (L3). At the end of the L3, the larvae cease feeding and leave the food looking for a site for pupation and become encapsulated in the pupal case. That is the beginning of metamorphosis, which occurs at ~120 hours AEL. Eclosion from the pupal case occurs at ~ 216-228 hours AEL and adult flies emerge. Although embryonic development lasts only 24 hours, it is a busy period of development. We chose to focus our assessments starting at stage 15 (Fig. 2) of development which corresponds to 12 hours AEL and 50% of embryonic development has taken place. At stage 15 the dorsal closure (process in which the dorsal epithelium reaches the dorsal midline) the central nervous system, the digestive tract and other systems are well underway (Campos-Ortega and Hartenstein, 1985). It is also at stage 15 when the 4 main protective membranes enclosing the embryo are fully formed. By stage 17 most tissues and systems are fully developed and coordinated muscle contractions are already taking place. The 4 protective membranes are lost when embryogenesis concludes after stage 17 at eclosion, when the larva leaves them behind. Once the embryo hatches, the L1 has fully developed mouth hooks and a highly branched tracheal system. The L1 will triple its size and in the next 32 to 48 hours as it reaches the L3 stage. Morphological features in terms of eggshell formation, digestive tract, neuromuscular system and tracheal system development not only serve as recognizable landmarks for stage identification, but also provide important structural integrity essential for both direct microtransfer and passive exposure assays presented here.

Eggshell formation

The eggshell membranes are (outward): the vitelline membrane (VM) of ~300 nm, the innermost chorionic membrane (IC) of 40-50 nm, the endochorion of 500-700 nm and the

exochorion of 300-500 nm (Fig. 3). The VM and the IC are both continuous but the IC is thinner. Researchers have also identified a multilayered wax between the VM and the IC. The endochorion and exochorion comprise a complex, multilevel structure, with cavities that allow exchange of substances (Margaritis, et al*.,* 1980).

Digestive tract development

Milestones in the digestive tract development are also important for staging. By stage 15, the midgut consists of 1 compartment which will continue to divide into 2 and 3 compartments in stage 16. By stage 17, the digestive tract is more convoluted and presents contraction in the visceral musculature (Fig. 2). Like humans, the *Drosophila* digestive system contains epithelial cells with secretory and absorption functions. Molecules involved in iron acquisition are conserved (Folwell et al., 2006). The Malvolio (Mvl) gene first identified by *Rodrigues* et al*., 1995*, and first implicate to metal transport by *Orgad* et al*., 1998*, is a homologue of the divalent metal transporter-1 (DMT1) which influences iron incorporation and homeostasis. This transporter protein is expressed in the gastrointestinal tissue and it is suspected to have a role in iron oxide (IO) nanoparticle internalization and further promoting nanotoxicity.

Neuromuscular junction development

Drosophila is currently one of the premier organisms for developmental studies (Thomson, 2004). Its neuromuscular system offers an accessible model nervous system suitable for studying the neuromuscular junction (NMJ) synapse (Thomson, 2004). The *Drosophila* neuromuscular network consists of a series of segmental repeats, an overall pattern of 30 overlapping fixed muscles in each hemisegment, which are innervated by 34 motor neurons extending from the central nervous system (CNS) (Keshishian et al*.,* 1996). The simple innervation ratio of motor neurons and their muscle partner contributes to the simplicity in the NMJ of *Drosophila* allowing for a precise developmental staging (Lnenicka and Keshishian 2000).

Drosophila as an *in vivo* testbed for toxicity assessment

Since *Drosophila* embryos and larvae posses a clear cuticle, we were allowed to validate a nanomaterial assessment by registering the developmental effects of nanomaterials in specific systems or individual cells of interest (Margaritis, et al., 1980). In order to quantify the effects of

nanomaterial exposure we focused mainly on the developmental milestones of the tracheal system, digestive tract, and motor neuron pattern. These systems have been previously described and are easily identified (Demerec, 1994; Hartenstein, 1993; Chiba, 1999; Keshishian et al., 1996). These developmental milestones allowed for quantification of overall mortality while identifying the specific stage of mortality.

Nanomaterials

Nanomaterials are structures of nanometer sizes, large surface area to mass ratio, and high reactivity (Singh et al., 2010). When in contact with biological fluids, the stability of the nanomaterials can be altered and their coatings could detach from the inorganic core. The core of these nanostructures can potentially induce intrinsic cytotoxic effects (Jain et al., 2008; Pisanic et al., 2003). Their increased propensity to diffuse across tissue barriers and biological membranes cause cellular stress and the possibility of tissue accumulation of free iron, in the case of iron oxide nanoparticles (Jain et al., 2008; Medina et al., 2007; Suh et al., 2009).

Today, researchers are able to synthesize and characterize nanostructures with biocompatible surface modifications to overcome cytotoxicity and magnetostatic attraction that take place between naked nanomaterials which leads to agglomeration and subsequent sedimentation (Singh et al., 2010). The final purpose of the nanomaterials needs to be considered when designing, synthesizing and choosing an assessment methodology. Parameters like magnetic behavior, monodispersity, size distribution, and composition homogeneity can be regulated by altering the synthesis' conditions (Gupta and Gupta, 2005; Singh et al., 2010). In the case of iron oxide (IO) nanoparticles, the magnetic behavior required is an important parameter to be considered in many biomedical applications and the synthesis reaction conditions, since it can increase or diminish the surface area, which will translate to different ranges of magnetization. Biomedical applications that employ the magnetic pull of IO nanoparticles (e.g. magnetic hyperthermia) usually require higher concentrations of nanomaterials.

The nanomaterials selected are present in everyday-use products or are employed for biomedical applications, and from which traces have been found in the environment. These are iron oxide (Fe_3O_4) (IO), silver (Ag), gold (Au), titanium dioxide (TiO_2), single-wall carbon

nanotubes (SWCNT) and multi-wall carbon nanotubes (MWCNT).

To assess nanotoxicity we employed Predicted Environmental Concentrations (PEC) in water calculated by Muellerand and Nowack, 2008 for TiO_2, Ag and CNT as our lowest concentrations for a realistic scenario. The PEC values were determined by a substance flow analysis from the products to the environment, waste incineration plants, landfills, and/or sewage treatment plants (Mueller and Nowack, 2008). We chose to employ the PEC value for water because of the possibility of nanomaterials spreading through the water cycle present bigger implications for environmental contamination. There is no data available on the PEC for Fe and Au (Norwegian Pollution Control Authority, 2008). PEC for iron has not been calculated since it is such an abundant element in the environment. For this reason, we decided to conduct our trials with the lowest employed concentrations at similar orders of magnitude to that of the ones established for TiO_2, Ag, and CNT. Our highest concentrations for IO nanoparticles were the initial concentrations at which our collaborators dilute the samples for other biomedical applications.

Iron Oxide

IO are typically spherical nanoparticles used as contrast agents for magnetic resonance imaging (MRI), in magnetic cancer hyperthermia and targeted drug or gene delivery. Iron is transported by transferrin, which in turn binds to a transferrin receptor, and once inside the cell is stored in proteins called ferritin. Concerns for the toxicity of IO nanoparticles have risen because it can be broken down into ferric ions that can reach high concentrations within the cell participating in the iron metabolism not being easily excreted (Soenen et al., 2011).

IO nanoparticles employed for this research were synthesized by two different methods. The first method consisted in the co-precipitation of aqueous iron solution (Fe^{+3}:$2Fe^{+2}$) in presence of a strong base resulting in the formation of small clusters of magnetic nanoparticles (Massart, 1981; Kawaguchi et al., 2001). The second method, thermo-decomposition of an iron-oleate in a high boiling point solvent, helped yield monodisperse nanoparticles with a narrow size distribution (Park et al., 2004). For this research three types of IO nanoparticles were synthesized by the Rinaldi Research Laboratory (University of Puerto Rico at Mayagüez); IO nanoparticles synthesized by co-precipitation with surface modifications of APS with either (1)

bond fluorescent succinimidyl-Alexa molecules and succinimidyl-poly(ethylene-glycol)-Biotin (Cop-IO-APS-Alexa-Biotin), or (2) CMDx (Cop-IO-APS-CMDx), as well as (3) thermo-decomposition followed by surface modifications by addition of APS and CMDx (Thermo-IO-APS-CMDx).

IO Surface modifications:

Coating nanoparticles with 3-Aminopropyltriethoxysilane (APS) or carboxymethyl-dextran (CMDx) is an example of the addition of a biocompatible coating, surface modifications. APS is an organosilicone coating reagent with two functional groups with different reactivity: one that reacts with organic molecules and one with inorganic materials. It is used to chemically add primary amines to a surface, which can be used to crosslink and immobilize molecules. APS is coupled to the surface, in this case the IO core, and the other compound of interest, if any, is coupled to the newly added amino groups. CMDx is a derivative of Dextran. It is used as a carrier for biosensor surfaces, as a stabilizer of proteins and biopolymers and as a stable non-toxic additive.

Commercially available nanomaterials

The nanomaterials used in these research- Ag, Au, TiO_2, SWCNT, and MWCNT were of commercial manufacturing. As bare nanomaterials these nanoparticles and carbon nanotubes aggregate and sediment in water. We found in the literature that colloidal stability of TiO_2 nanoparticles improves when suspended in a solution of 10% fetal bovine serum (FBS) or 1% human serum albumin (HSA) (Allouni et al., 2009). We decided to suspend our nanomaterials in 10% bovine serum albumin solution (BSA 10%). This resulted in well-suspended nanomaterial solutions that allowed for microinjection protocols without clogging the microneedle.

Silver and gold:

Nanotoxicity research has been mainly conducted with Au and Ag nanoparticles because both are widely used and present an increased potential of human exposure (Johnston et al., 2010). Hussain et al. (2001), Hillyer and Albrecht (2001), and Tkachenko et al. (2004) have all independently shown the capability of unconjugated Au nanoparticles to pass through cellular and nuclear membranes. Also, because the optical resonance spectrum is in the visible range, Au nanoparticles make excellent optical markers for evaluating cellular uptake and tissue

distribution (Johnston et al., 2010). On the other hand, Ag's antimicrobial properties have been exploited in many products (e.g. clothing) but it is still unclear if the toxicity excerpted to microorganisms is due to the nanoparticle size and/or the release of Ag ions (Lubick et al., 2008). From a toxicity point of view, Ag nanoparticles have been linked to cytotoxic, oxidative, genotoxic, and inflammatory effects; and both, Ag and Au nanoparticles have shown to accumulate in the liver (Johnston et al., 2010).

Titanium dioxide:

TiO_2 is contained in sunscreens and because of its photoinstability can generate free radicals that have been linked to DNA mutations (Ostiguy et al., 2006). The most common exposure routes for TiO2 nanotoxicity assessments are inhalation and dermal exposure. TiO2 used to be considered nontoxic and served as a control in many studies (Ostiguy et al., 2006). *Hohr* et al. *2002*, as others before them, showed that TiO_2 triggered early parameters of inflammation after inhalation, and concluded that particle surface is the determining factor. In terms of dermal exposure, while some researchers suggest a low probability of cutaneous absorption (Schulz et al., 2002; Lademann et al., 1999), others indicate a health risk after a prolonged exposure (*Wu* et al*., 2009*). *Wu* et al*., 2009* presented *in vivo* data demonstrating TiO2 nanoparticle absorption with a wide organ distribution and that TiO2 nanoparticles induce skin aging from a collagen perspective.

Carbon nanotubes:

CNT are hexagonal cylinders of carbon atoms having diameters from 0.7 to several millimeters, multilayered nanotubes reaching up to 20 nm (Ostiguy et al., 2006). CNT can be single wall carbon nanotubes (SWCNT) or multi wall carbon nanotubes (MWCNT) and are chemically and thermally stable. CNT are being used in electromagnetic shielding, as polymer composites for hydrogen storage, and in batteries (Ostiguy et al., 2009). Both SWCNT and MWCNT have shown to be internalized and accumulated in cells, reducing cell viability through different mechanisms (Pantarotto et al., 2004; Monteiro-Riviere et al., 2005). In a comparative study of cytotoxicity on alveolar macrophages in guinea pigs SWCNT showed higher toxicity than MWCNT (Jia et al., 2005).

As general findings, toxicity effects can be adjudicated to smaller nanomaterial size

and/or particle dissolution. A combination of both is plausible but the current data is insufficient and little consensus has been reached. This is mostly due to differences in *in vitro* and *in vivo* models, differences in exposure routes and duration of exposure, and the differences in nanomaterial size and surface modifications. Our validated cost-effective product-specific science based nanomaterial assessment using *Drosophila* as an *in vivo* model will allow researchers to establish toxicity effects as function of particle size, and presence or not of surface modifications with two different interaction routes.

CHAPTER III

MATERIALS AND METHODS

Pre-assay preparations

IO Nanoparticles

Our collaborators from the Rinaldi Research Laboratory at the Chemical Engineering Department of the University of Puerto Rico at Mayagüez synthesized the IO nanoparticles employed in these trials. The employed concentrations of the IO nanoparticles were: 7.0E-07 µg/mL, 7.0µg/µL, 20 µg/µL, 30 µg/µL and, 54 µg/µL. The chemical synthesis of each is described below:

Iron oxide (IO) magnetic nanoparticles coated with amino-propyl-silane (APS), Alexa, and NHS-PEG-Biotin (Cop-IO-APS-Alexa-Biotin):

46 nm IO-APS-CMDx-Alexa-Biotin are synthesized by co-precipitation of aqueous iron solution (Fe^{+3}:$2Fe^{+2}$) with ammonium hydroxide at 80 °C and pH 8.0 (Massart, 1981). Nanoparticles were cooled to room temperature, peptized with tetramethyl ammonium hydroxide (1 M) and dried at 65°C in a vacuum oven. After being suspended in dimethyl sulfoxide (DMSO) at 0.75 % w/v using an ultrasonic bath, functional amine (NH_2) groups were grafted onto the magnetic nanoparticles surface by using the silane-amine molecule 3-Aminopropyltriethoxysilane (APS), which was attached onto the surface of the magnetic nanoparticles by the hydrolysis/condensation mechanism in the presence of acetic acid (Herrera, 2008a). Functional amine groups were used to covalently bond fluorescent succinimidyl-Alexa molecules (Invitrogen; Carlsbad, CA) and succinimidyl-poly(ethylene-glycol)-Biotin (ChromaLink; SoluLink, San Diego, CA) onto the IO nanoparticle surface. APS coated magnetic nanoparticles were suspended in deionized water at 1 mg/ml and at pH 4.0 and 5 ml of the colloid suspension was reacted with 35 l of a solution of succinimidyl-poly(ethylene-glycol)-Biotin prepared at 0.095 mM. After stirring at 250 rpm for 1 hour, 0.25 ml of succinimidyl-Alexa solution prepared at 1.2 mM were added and the reaction was carried out for another 1 hour at 250 rpm. Free succinimidyl-Alexa and PEG-Biotin molecules were removed using centrifugal filter units with 30 kDa MWCO at 3400 rpm.

Iron oxide (IO) magnetic nanoparticles coated with carboxymethyl-dextran (CMDx) synthesized by co-precipitation (Cop-IO-APS-CMDx):

76 nm IO magnetic nanoparticles were synthesized by the co-precipitation method and coated with APS molecules as described above. Subsequently, nanoparticles were functionalized with CMDx using carbodiimide chemistry (Herrera, Barrera, Rinaldi, 2008a). 0.1 g of IO-APS nanoparticles were suspended in 10 mL of deionized water at pH 5.0 and reacted with an aqueous solution of CMDx prepared at 20 %w/v with the addition of 25 mg of 1-ethyl-3-(3-dimethylaminopropyl) carbodiimide hydrochloride (EDC) and 15 mg of N-hydroxysuccinimide (NHS). The reaction was carried out at room temperature for 24 h and then the functionalized nanoparticles were washed three times with ethanol and dried at room temperature.

Iron oxide (IO) magnetic nanoparticles coated with carboxymethyl-dextran (CMDx) synthesized by thermo-decomposition (Thermo-IO-APS-CMDx):

40 nm single iron oxide (IO) magnetic nanoparticles were synthesized by the thermal decomposition method (Park *et. al.*, 2004). To obtain Thermo-IO nanoparticles an iron-oleate solution was first prepared by reacting iron (III) salt with sodium oleate in a mixture of water/ethanol/hexane (1:1:2) for 4 hours at 70 °C (Barrera et al., 2009; Park *et. al.*, 2004). 25 g of the iron-oleate solution was reacted with 100 ml of 1-octadecene and 2 g of oleic acid at 320 °C for 1.5 hours. Synthesized nanoparticles were washed with anhydrous ethanol, suspended in hexane at 45 % v/v for subsequent ligand exchange between oleic acid and then reacted with 6 mL of APS in presence of 50 mL of acetic acid. Afterwards, the reaction mixture was mechanically stirred at 150 rpm for 72 hours and finally, APS coated Thermo-IO nanoparticles were modified with CMDx as described above.

IO nanoparticle characterization:

The hydrodynamic diameters of the functionalized nanoparticles were measured using a Brookhaven Instruments BI-90 Plus particle size analyzer (Brookhaven Instruments; NY, USA). For these measurements nanoparticles were suspended in distilled water and then filtered with 0.2 μm nylon filter syringes. The size was determined by Transmission Electron Microscope (TEM) using a JEOL 1200EX (JEOL; Tokyo, Japan). The ImageJ program (ImageJ; US National Institutes of Health, Bethesda, MD, USA) was used to measure the diameters of the

magnetic nanoparticles.

Commercially available nanomaterials

The employed concentrations for Ag nanoparticles were: 3.0E-08 µg/mL, 3.0E-04 µg/mL, 0.03 µg/µL, and 3.0 µg/µL. The Ag nanoparticles have a diameter < 90 nm and purity of 99.9% (MKnano; Mississauga, Canada). Au nanoparticles were used at the following concentrations: 7.0E-07 µg/mL, 7.0E-04 µg/mL, 0.07 µg/µL, and 7.0 µg/µL. Au nanoparticles have a diameter of <150 nm and purity of 99.9% (Sigma-Aldrich; MO, USA). The concentrations for TiO_2 nanoparticles were: 7.0E-07 µg/mL, 0.07 µg/µL, 3.5 µg/µL, and 7.0 µg/µL. The TiO_2 nanoparticles (Degussa P25) have a diameter < 20 nm and purity of 99.9% (MKnano; Mississauga, Canada). The concentrations for CNT were: 5.0E-10 µg/mL, 5.0E-04 µg/mL, 0.05 µg/µL, and 5.0 µg/µL. The SWCNT have an outer diameter of 1-2 nm, an inner diameter of 0.8-1.6 nm, length of 5-30 µm, a surface area of 407 m^2/g and purity > 90wt% (Cheap Tubes, Inc.; VT, USA). The MWCNT have an outer diameter < 8 nm, an inner diameter of 2-5 nm, length of 10-30 µm, a surface area of 500 m^2/g and purity > 95wt% (Cheap Tubes, Inc.; VT, USA).

Embryo collection

Male and female Canton S wildtype *Drosophila* flies were maintained at 25ºC and 60% RH in embryo collection chambers for at least 2-3 days prior to experimentation. Different cages have been previously described and any are suitable for the task (Featherstone, Chen and Broadie, 2009). All cages consist of a vial that allows for air exchange (either perforations or a 97 µm mesh) on one side and a Petri dish containing egg-laying media on the other. Instead of the usual 100 x 20 mm for embryo collection, we chose to use 35x10 mm Petri dishes to increase the possibilities of mating. The egg laying media recipe was modified from the Bloomington *Drosophila* Stock Center (1998) [550 mL Welch's concentrated grape juice, 170 mL H2O, 43 g glucose, 21 g sucrose, 18 g agar, 24 mL 1N NaOH, 1.28 g Calcium propionate, 320 uL phosphoric acid]. Instead of harvesting timed embryo collection, in which fresh egg-laying agar plate is exposed to adult flies for two hours and allowed to continue to develop for an additional 11 (to obtain embryos around stage 15), 24 h embryo collections were allowed. That way the embryos collected would be in almost every stage of development, providing enough embryos to work with for at least 8 h by correctly staging the embryos following the morphological signs

previously explained in the literature review.

Tissue-Specific Nanomaterial Assessment:

Direct Microtransfer Interaction Route

Glue preparation

The glue was made beforehand by dissolving ~2.5cm of 3M double-sided clear polyester with 400 High-Tack Acrylic (type 415) (3M Industrial Adhesives and Tapes Division; MN, USA) in ~1ml heptane in a tightly capped glass vial. In order to dissolve the glue part of the tape the vial was placed in a Vortex at maximum speed for 15-30 minutes. Finally, the polyester adhesive carrier was removed. This tape offers good temperature and humidity resistance and is advertised to offer a good balance between initial adhesion and long-term holding power.

Embryo preparation

Collected embryos were dechorionated (removal of chorion membrane) while monitored under an Olympus MVX10 MacroView (Olympus; PA, USA) stereomicroscope following a previously explained dechorionation protocol (Featherstone, Chen and Broadie, 2009) with fresh 50% bleach but only for 2 minutes (instead of 5 minutes) to ensure the other membranes were left intact. A micro probe and a brush with a fine tip allowed us to precisely handpick embryos and to properly orient them according to experimental needs (Fig. 4A). Embryos were selected according to the standard embryonic development in *Drosophila* (Campos-Ortega and Hartenstein, 1985), as previously described above, at 12 hours AEL. Embryos were mounted with their lateral side facing down over a smooth, even-surfaced egg-laying agar piece, aligning embryos so that the posterior end is easily accessible to the microneedle, in this case to the right (Fig. 4B).

A coverslip sandwich was prepared consisting of a clean 5 x 5 mm coverslip over a clean 22mm diameter circular coverslip. Placing one to two drops of tape glue over the square coverslip and allowing excess to flow over the edges and air dry. This effectively created a secure mounting surface for the embryo, which can be easily aligned to the microneedle during microinjection steps, ensuring a consistent embryo penetration and an easy removal after experimentation to be placed in a recuperation chamber. The glue-covered coverslip side was gently lowered and pressed, to pick up embryos from the agar making sure embryos were placed

towards the center of the coverslip and that they remained aligned as it is impossible to rearrange after they are in contact with the glue. A drop of halocarbon oil series 700 (Halocarbon Products Corp.; NJ, USA) was used to cover the embryo and minimize dehydration during subsequent steps. Finally, the coverslip sandwich was placed in appropriate circular coverslip holders (Fig. 4C). A custom-made round coverslip holder was used to fit the microscope stage although there are commercially available holders and mounts suitable to a different microscopy setup.

Microneedle parameters, installation and loading

Prior to embryo preparation multiple parameters were established. Optimal microneedle equalized atmospheric pressure (EPA) to prevent unwanted loss/leakage of nanomaterials while the needle is suspended in midair, the Equalized Pressure in Halocarbon Oil (EPO) to prevent unwanted suction loss/leakage of nanomaterials in halocarbon oil and the Nanomaterial Transfer Value (TrV). Each of these parameters were predetermined in preliminary trials for every solution to be transferred into the embryo by observing the behavior of the different solutions inside the Eppendorf TransferTip-R (ICSI) (Eppendorf; Hamburg, Germany) microcapillarie when in halocarbon oil, inside the embryo or by itself. The TransferTip-R (ICSI) microcapillarie (microneedle) with 35° angle at the microneedle's tip was mounted in a XenoWorks system (Sutter Instruments; Novato, CA) consisting of a digital micromanipulator that works together with a XenoWorks micromaninjector MP-285 as per manufacturer's instructions (Fig. 5).

Using an Olympus IX81 (Olympus; PA, USA) inverted microscope with Volocity 5.3 (PerkinElmer; MA, USA) imaging software and a Hamamatsu Orca ER camera with FireWire Interface (Hamamatsu Photonics, Hamamatsu City, Japan), and a low-power objective the microneedle's tip was located and focused. Afterwards, the needle was raised out of the way and the coverslip holder was mounted with a clean 22mm diameter coverslip. A drop of 5 μL of the nanomaterial solution was placed over the coverslip and loaded into the microneedle by altering transfer values of the microinjector for suction. The microneedle was raised out of the way as we returned to the predetermined EPA and the 22mm diameter nanoparticle-containing coverslip was removed.

Nanoparticle microtransfer

The embryo-containing coverslip and holder were placed in the microscope and the

coverslip rotated so that the posterior end of the embryo was parallel to the microneedle. The specimen was located, focus was adjusted and images prior to microtransfer were acquired. Epifluorescence and confocal imaging could be conducted if the organism or the nanomaterial solution has a fluorophore. Pressure value was increased up to the EPO and the microneedle was immediately lowered into halocarbon oil. The microneedle was placed close to the posterior end of the embryo, focus adjusted and embryo and/or microneedle realigned as necessary. The microneedle was moved in the X-axis to puncture the embryo in a single, controlled motion and stopping at the intersegmental boundary of the 5th and 6th abdominal segments (A5 and A6) (Fig. 6). With our settings and equipment, EPO is also the TrV necessary pressure for microtransfer, which is why immediately after reaching the A5/A6 boundary the microneedle was retracted.

The tip of the needle could be damaged or clogged after a few injections. Care must be taken to exchange the needle whenever necessary. We tested microneedle viability in our preliminary trials by measuring how many microtransfers into an embryo could be conducted without clogging the needle or damaging the tip. For which we decided to change the needle every 25 microtransfers. The microneedle was raised out of the halocarbon oil and the TrV lowered to EPA to minimize loss of solution. Images were acquired after focusing the embryo.

Embryo recovery

In a fresh egg-laying agar plate, a piece of approximately 10mm x 10mm was cut and filled with dry yeast paste. Using forceps, the small 5x5 mm embryo-containing coverslip was detached by scraping the tape glue off of the edges and separating it from the 22mm diameter coverslip. Four embryo-containing coverslips were placed inside each egg-laying agar plate at each side of the yeast (Fig. 7A) and each agar plate inside a recovery chamber and kept at 25ºC and 60% RH (Fig. 7B). Each chamber was covered with aluminum foil to minimize light exposure and embryos were allowed to continue development for 48 hours.

After 48 hours the 5x5 mm embryo-containing coverslip were taken from the recovery chamber and placed over a 22 x 50 mm cover slip for imaging. Images were taken to register the stage of development after 48 hours. Normally, development into first instar larva takes approximately 24 hours, to second instar larva, 48 hours and to third instar larva, 72 hours. For

additional information regarding larval development refer to Literature Review.

The assay was conducted with experimental trials for each nanomaterials at different concentrations (n = 50), with 3 control trials: insect saline (n = 50); to account for the mortality caused by mechanical damage of puncturing the embryo, water (n = 50) and BSA 10% (n = 50); to account for the mortality caused by the liquids the nanomaterials were suspended in.

Volume quantification

Before mounting the microneedle, a thin piece of electrical tape was placed around the outer surface of its thickest part to create an initial marking. The microneedle was mounted in the micromanipulator/microtransfer device and the loading protocol explained previously was conducted allowing the meniscus to be as close as possible to the electrical tape mark but leaving some space. Without disconnecting the microneedle from the micropipette holder or pressure tubing of the microinjector, the micropipette holder was placed in a horizontal position inside of a holder of our own making. This holder kept the micropipette and pressure tubing on the microscope stage in a horizontal position over the objective allowing us to capture images of the spacing between the meniscus and the tape always showing booth barriers (Fig. 8). An initial image was acquired before microtransfer (x_0).

After 5 microtransfers the microinjector was taken out of the micromanipulator and placed into the holder to acquire an image of the spacing between meniscus and tape. This was repeated 5 times (25 microtransfers) to average the results. Using Volocity as image analysis software, the lengths from the meniscus to the tape were determined. The injected volume was determined using the cylinder volume formula ($V = \pi r^2 h$), where "r" is the internal radius of the microneedle and "h" is the measured lengths determined from the images acquired. For instance, the length is equal to the difference between the initial mark (x_0) and the next mark after "n" microtransfer (x_n). The equation can therefore be written as: $V = \pi r^2 (x_1 - x_2) / n$. Knowing the volume transferred into the embryo and the initial concentration of the nanomaterial solution, it was possible to quantify the amount of nanomaterials inside an embryo.

Dosage extrapolation

An extrapolation based on body surface area comparison was conducted. The body surface area of a *Drosophila* embryo was calculated through a simple formula based on a prolate

spheroid, a body equivalent ellipsoid by Reading and Freeman, 2005. (SA) = 4πac, c = H/2, H = height = 500 μm, a = minor axis = 75 um. SA= 2.36 x 10^{-7} m^2. Human SA was calculated by averaging the values obtained from 5 of the main equations for body surface area of a human (DuBois and DuBois, 1916; Gehan and George, 1970; Haycock et al., 1978; Mosteller, 1987; Reading and Freeman, 2005). A conversion factor between embryo and human SA was calculated ((human SA)/(embryo SA)). The amount of nanomaterials per human dosage was calculated by applying the conversion factor to the amount of nanomaterials per embryo dosage. The equivalent microtransfered volume in a human was also established by applying the conversion factor to microinjected volume in an embryo. Dosage (μg/m^2) = ((amount of nanomaterials per microtransfer) / (SA)).

Statistical analyses

In order to establish the significance of our data statistical analyses were conducted. Data distribution was assessed through the Shapiro-Wilk test. The null hypothesis of the Shapiro-Wilk test is that the data is normally distributed. For this test we choose the statistical level of significance (α) to be 0.05. The test yields a W value which is the p-value and if $p < \alpha$ the null hypothesis is rejected. Once we noticed the data was not all normally distributed we conducted a non-parametric analysis, a Fisher's exact test. This test allowed us to determine if 2 binary proportions (categorical data) are equal or different when our samples are independent. Its null hypothesis establishes that there is no difference between the two proportions. For this test we also used $\alpha = 0.05$. The test yields a p-value and if $p < \alpha$ the null hypothesis is rejected.

Passive Transport Nanomaterial Assessment: Direct Contact-Exposure Route

Embryo preparation

Embryos were harvested from a timed collection chamber, unlike the tissue-specific assessment, and fresh egg-laying agar plate exposed to adult flies for two hours and allowed to continue to develop for an additional 11 hours at 25ºC and 60% RH. The embryo collecting plate was gently rinse with ddH_2O and drained through a mesh.

Nanomaterial exposure and internalization

The mesh was place in an aluminum foil-covered petri dish and 30 μL of nanomaterial

solution was added over embryos. Nanomaterials employed were the same as in the tissue-specific assessment except SWCNT and MWCNT were not tested. Bare CNT without any inorganic trace metals cannot be identified through ICP-MS. We expected to quantify the internalized trace metals through ICP-MS analysis. Embryos remained in contact with the nanomaterial solution for 3 hours and then rinsed gently with ddH_2O. The group of embryos was divided in 2 batches after the 3-hour incubation. One batch was left intact: without removing the chorion membrane, and the other had their chorion membranes removes by the bleach-mediated dechorionation protocol previously explained. 2 groups of 50 embryos from the intact batch, and 2 from the batch without chorion membrane were formed. Each of the 8 groups was digested in 200 µL of nitric acid for 1 hour at 100°C and then diluted in 1/50 of deionized H_2O to be analyzed through ICP-MS to measure nanomaterial traces. ICP-MS analyses were conducted by Pace Analytical Services, Inc. (Pace Analytical, Inc., St. Rose, LA, USA). Other than the experimental trials with 6 nanomaterials at 2 concentrations each, this protocol was conducted with a group of embryos that were not in contact with nanomaterials and by digesting H_2O, BSA 10%, insect saline and egg-laying agar separately.

CHAPTER IV

Figures

Figure 1

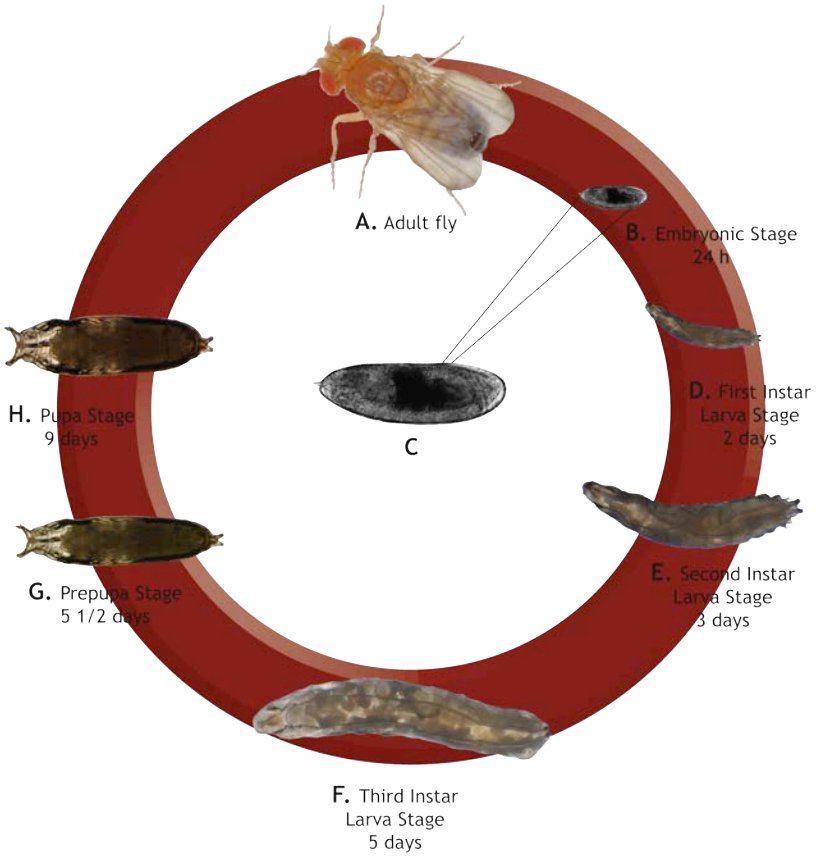

***Drosophila* Life Cycle.** All stages of the *Drosophila* life cycle are readily accessible and amenable to manipulation with a variety of basic to high-end tools and techniques. Imaging techniques can be conducted in every stage of development (A-H) thanks to the clear cuticle during embryonic (B-C), larval (D-F) and partially during pupal (G-H) and adult stages (A). Flies (A) lay their embryos (B). Embryos hatch into first instar larva (L1) (D). L1 molts into second instar (L2) (E), and L2 into third instar larva (L3) (F). (C) Is the enlarged photo of a stage 15 embryo.

Figure 2

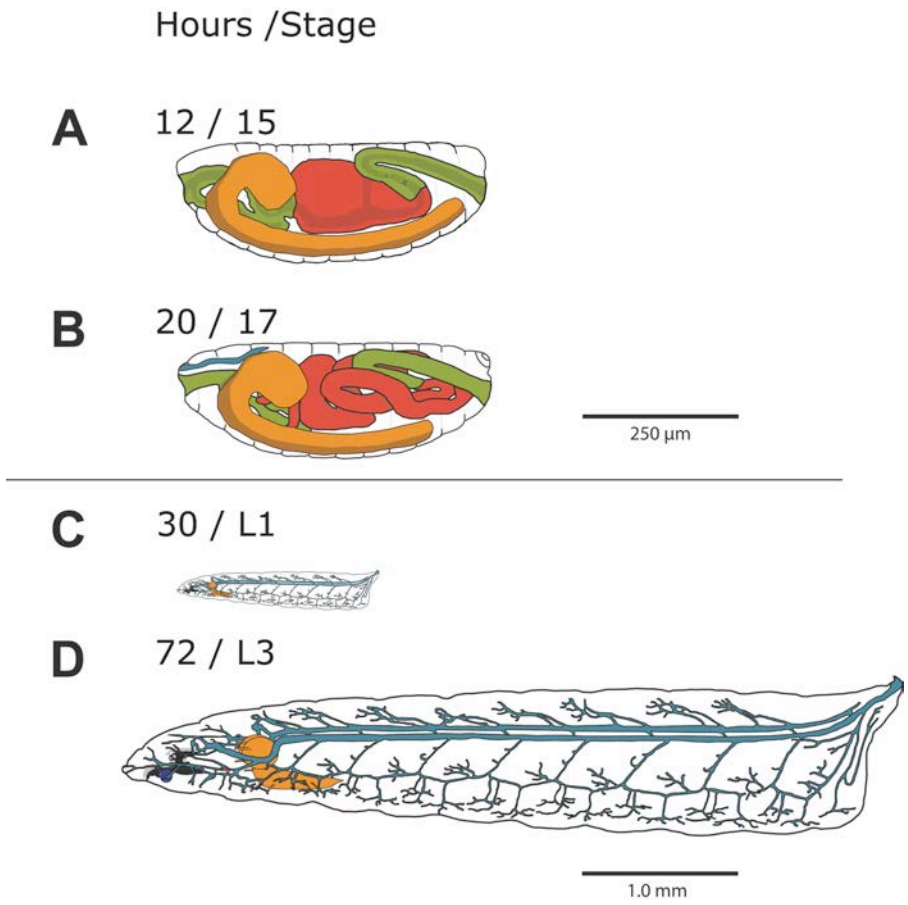

Embryonic and Larval Development (Diagrams). Approximately 12 hours AEL, embryos reach stage 15 (A), which corresponds to 50% of completed embryonic development. By this stage, central nervous system (CNS) (*orange*), digestive tract (*green and red*) as well as many other systems (*not shown*) are well underway (for a detailed review, please see Campos-Ortega and Hartenstein, 1985). The CNS consists of 2 lobes that form the central brain and a ventral nerve cord. Thanks to the shortening of the ventral nerve cord the CNS is not harmed when the embryo is microinjected from the posterior side. *Drosophila*'s digestive tract or gut is composed of three parts, the foregut (anterior *green*), midgut (*red*) and hindgut (posterior *green*). In stage 15 the midgut has 1 compartment that divides into 2 during late stage 15 (A). By stage 16 (*not shown*) the midgut is divided into four compartments by three constrictions. By stage 17 these compartments form a more convoluted midgut tube, retraction of the ventral nerve cord continues, muscle contractions are already taking place and the trachea system is fully developed (*blue, shown in part*) (B). The tracheal system is somewhat omitted in the stage 17 embryo to give more emphasis to the digestive tract, but it would be organized in the same way as in the L1 (C). L1 has fully developed mouth hooks and tracheal system. In the next 32 to 48 hours L1 will molt into L3 (D). Digestive tract and other systems are omitted in larval stages (C-D) to give more emphasis to tracheal system.

Figure 3

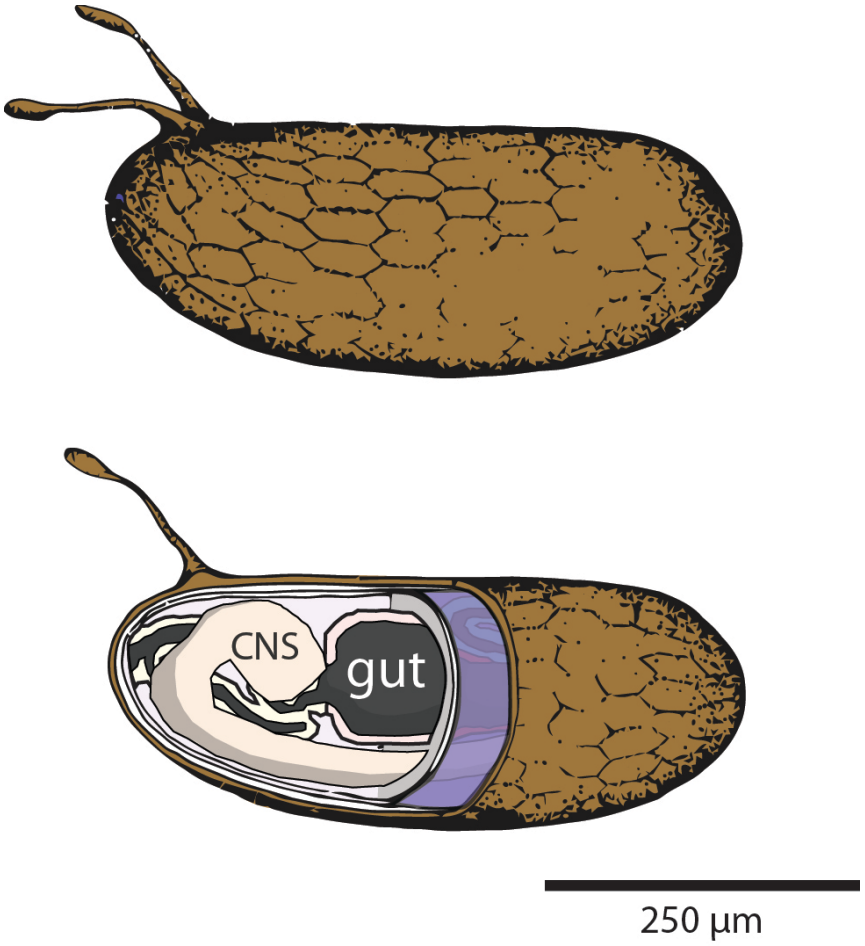

Eggshell membranes (Diagrams). (A) Embryo with intact chorion membrane (*purple*). (B) Cutout view of an embryo to demonstrate the membrane organization over the embryo surface: chorion membrane (*purple*) and vitelline membrane (*brown*). Mayor systems, like the CNS and gut, can be seen through the vitelline membrane when the chorion is removed. Other structures seen in late embryogenesis can also be seen through the vitelline membrane like mandibular buds (md), malpigian tubes (mt), and spiracles (small entry to allow air to enter the tracheal system) (*not shown*).

Figure 4

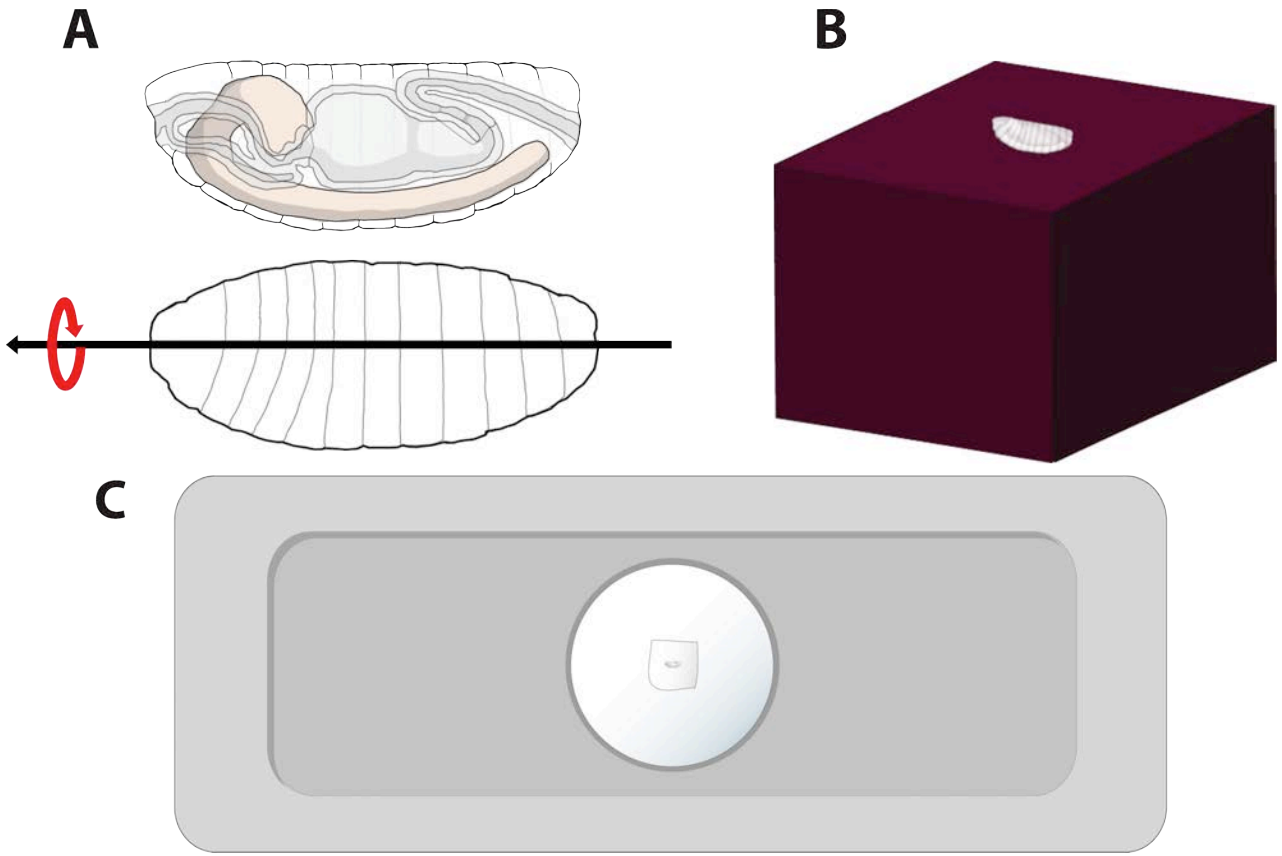

Embryo mounting procedure. (A) The embryos are oriented with their lateral side facing down. (B) Embryos are oriented over a smooth, even-surfaced egg-laying agar piece. It is imperative to align embryos so that the posterior end is easily accessible to the microneedle in your setup, in our case posterior side facing right. (C) Coverslip and coverslip holder. The embryos are gently transferred over a glue-covered coverslip and a drop of halocarbon oil is placed over and the coverslip placed over the coverslip holder.

Figure 5

Microscope, micromanipulator and microinjector setup. XenoWorks Digital Microinjector together with a right-hand XenoWorks Micromanipulator MP-285 mounted in an Olympus IX81 inverted microscope. Using digital microinjection and micromanipulation equipment assures the precision of the microtransfer.

Figure 6

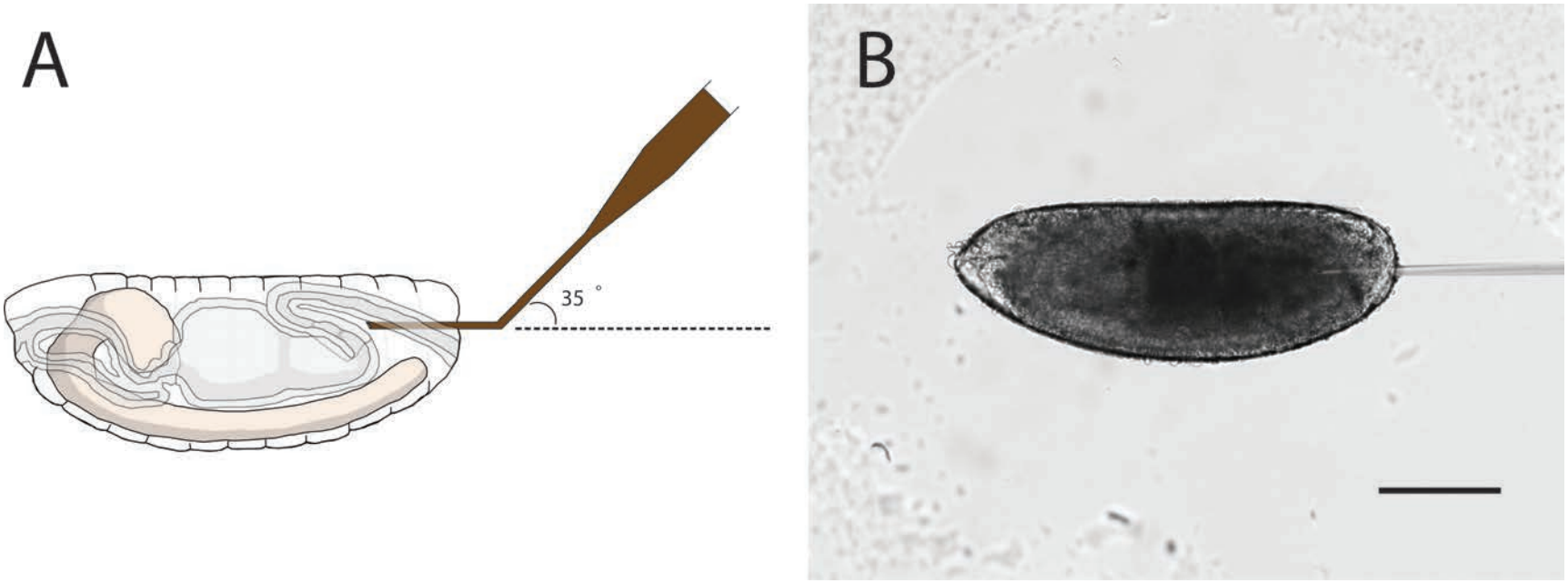

Embryonic microtransfer procedure. (A) Diagram. (B) Live imaging. The Eppendorf TransferTip-R (ICSI) has a 35° and the microtransfer is conducted at the intersegmental boundary of the 5th and 6th abdominal segments (A5 and A6). Scale bar = 140µm.

Figure 7

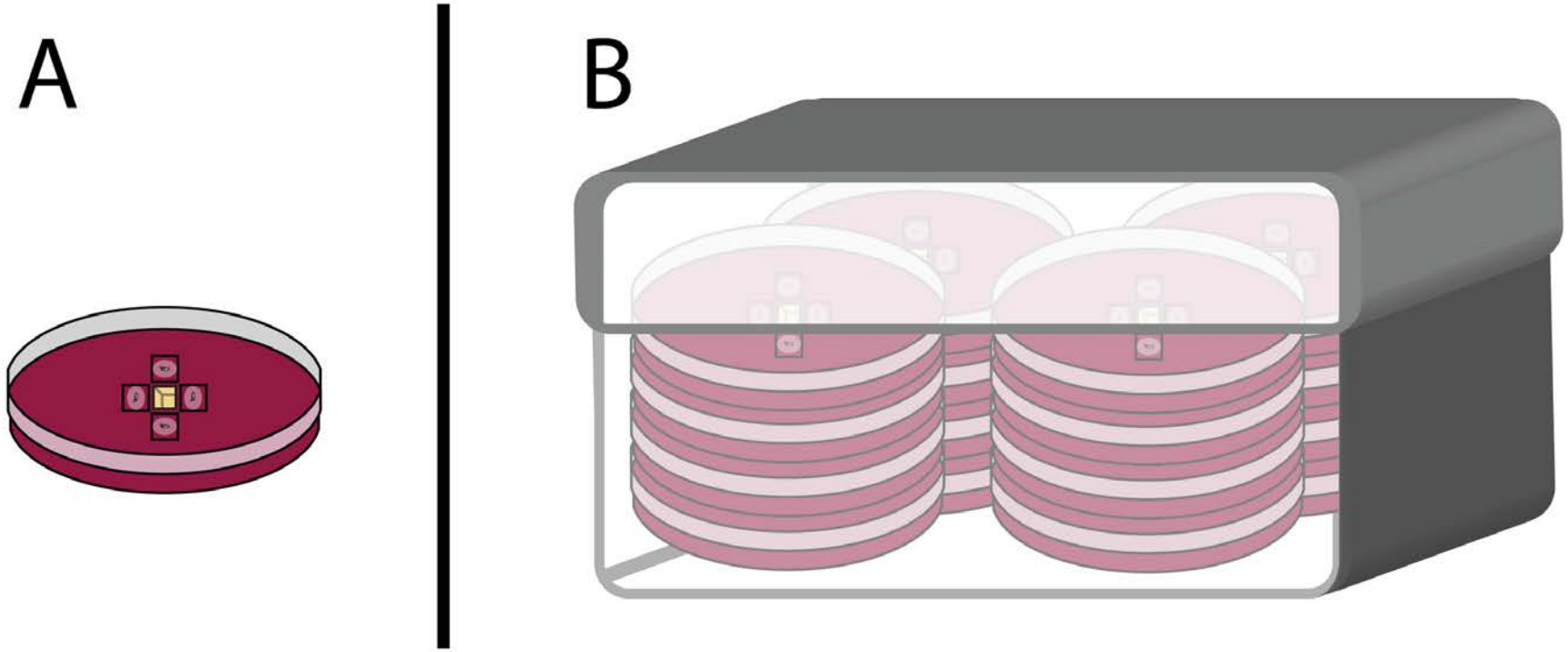

Post-injection Recovery. (A) Recovery plate: egg-laying agar plate with embryo-containing coverslips surrounding a small well with yeast paste. (B) Recovery chamber: kept at 25ºC and 60% RH.

Figure 8

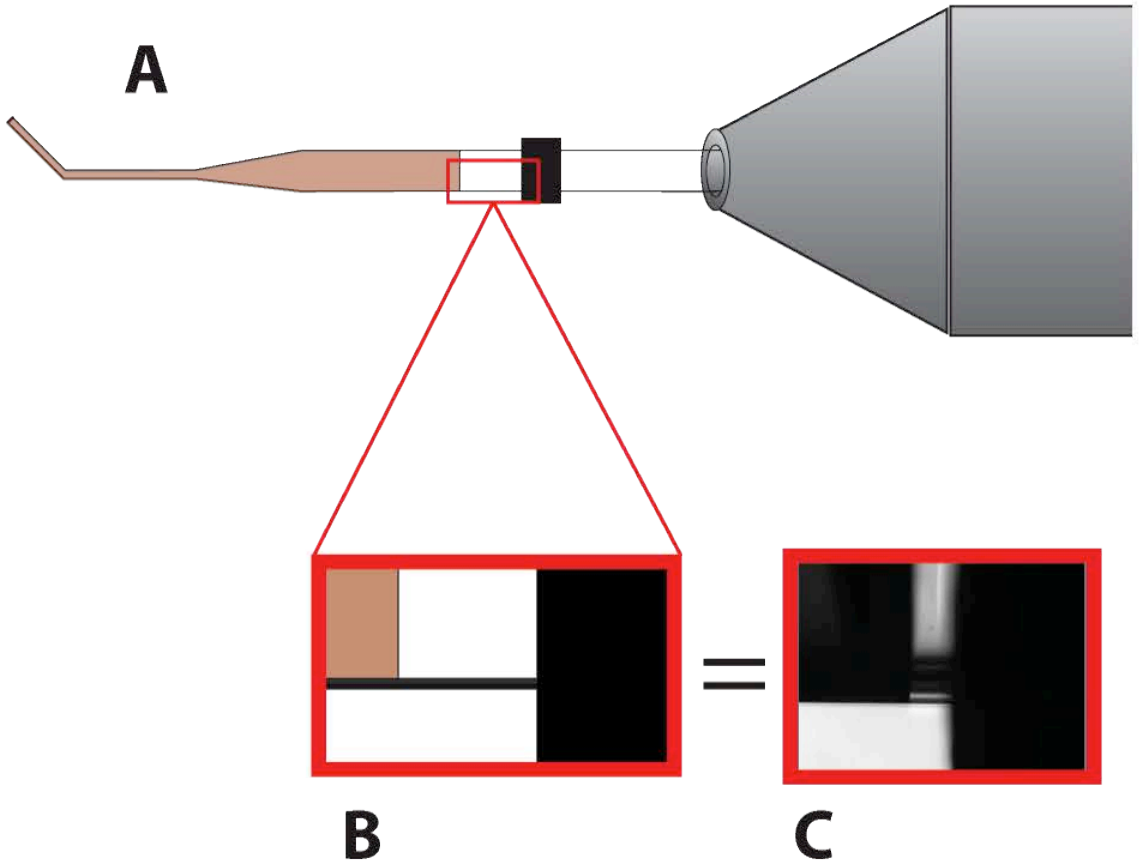

Microneedle visualization procedure. (A) Needle still attached to the microinjector emphasizing the spacing between the meniscus and the tape to measure volume displacement after microtransfers. (B-C) Diagram and actual image of the spacing between the meniscus and the tape.

Figure 9

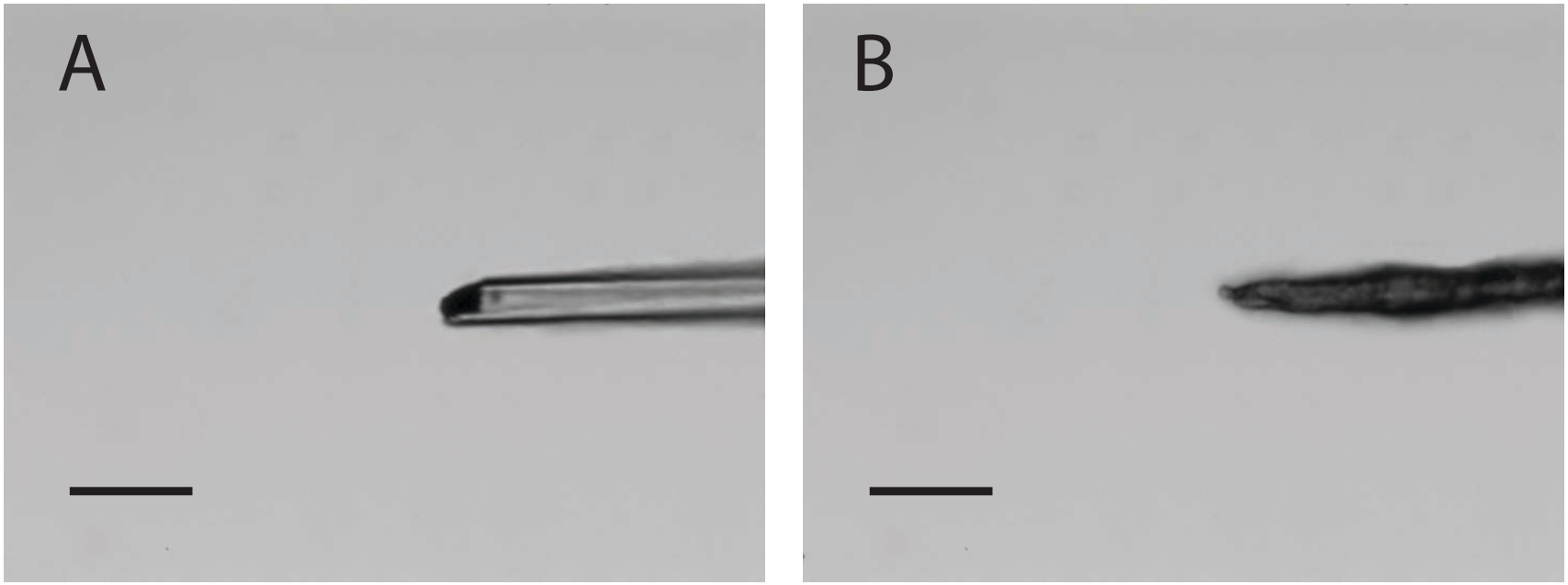

Laboratory-made microneedles. (A) Broken needle tip will assure high mortality rates as the internal organs will most likely get out of the embryo from the microneedle entry. (B) Nanomaterial solution affinity to microcapillary material clogs the needle and injected volumes will vary from one injection to the next. Scale bar = 140µm.

Figure 10

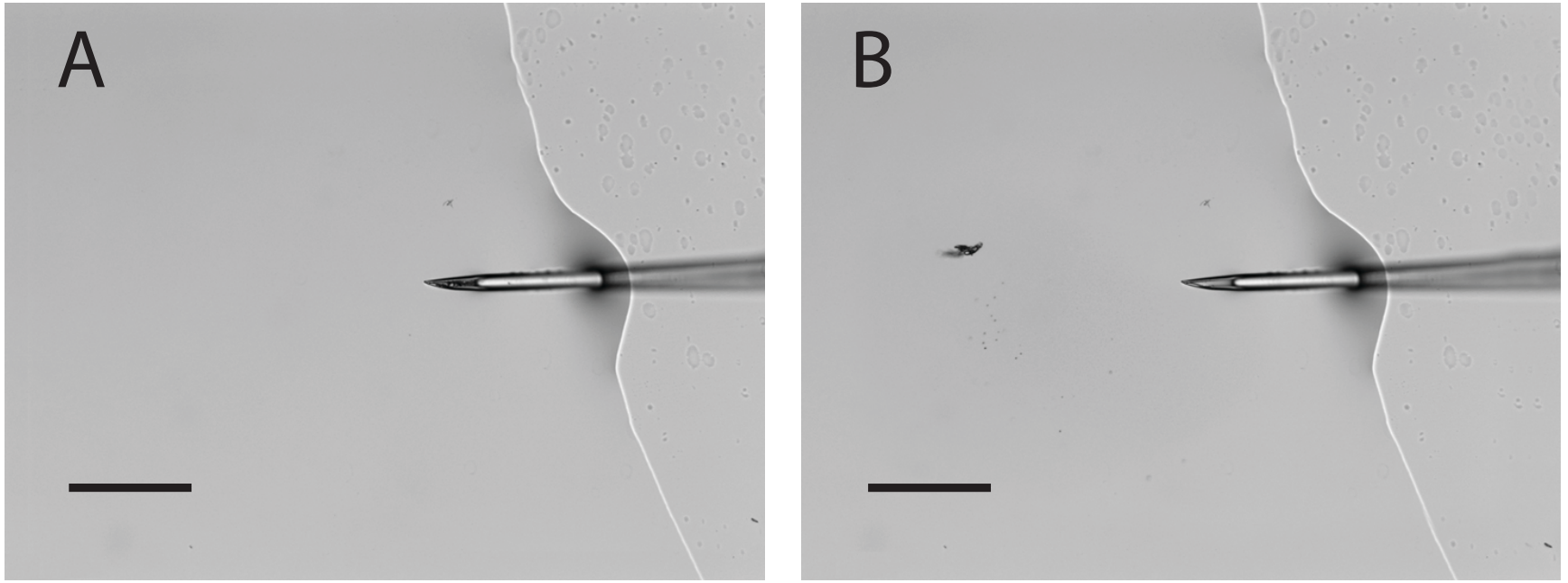

Microneedle Troubleshooting. (A) Clogged microneedle by glass debris or nanomaterials will lead to higher transfer values for microdelivery. (B) To Unclog a microneedle high values of pressure are needed (i.e. 502hPa of pressure and +020 transfer value). Scale bar = 140µm.

Figure 11

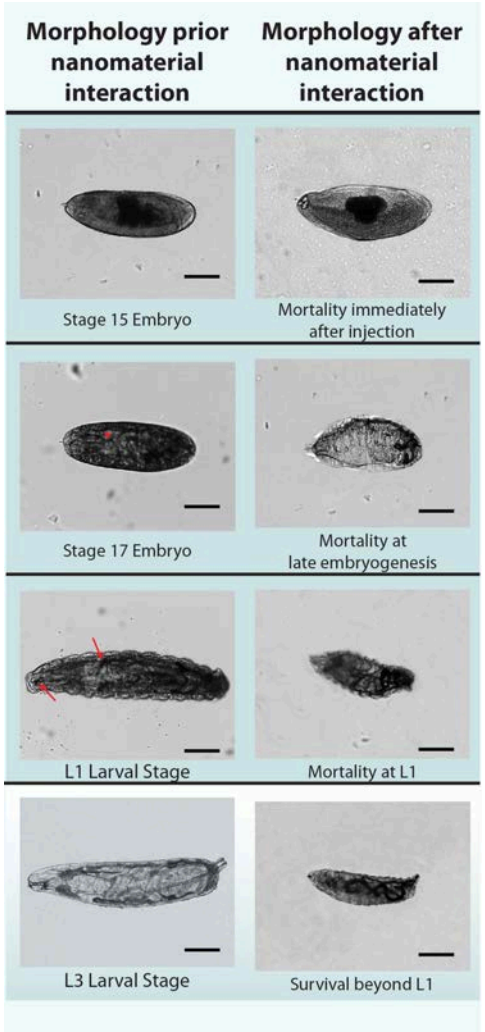

Morphology Prior and After Nanoparticle Interactions through Direct Microtransfer. (B) Mortality immediately after injection: in which embryonic development did not progress past stage 15. Degradation of tissue is observed when compared to a (A) healthy stage 15 embryo. (D) Mortality at late embryogenesis: characterized by progression towards late embryogenesis (stages 16 and 17), with tracheal system development (arrowhead in Fig. C) and muscle innervation apparent, but failed to progress to first instar wandering larval stages (not shown). Degradation of tissue is observed when compared to a (C) healthy stage 17 embryo. (F) Mortality at L1: characterized by fully developed L1 development, but failed to progress to later developmental stages. These individuals showed a developed tracheal system and mouth hooks (arrows in Fig. E), but exhibited no locomotion and no visceral musculature contractions. (H) Survival beyond L1: characterized by survival beyond the L1 stage, including the L2 and L3 stages. Scale bars = (A-F)140µm, 1mm (*G*) and 200µm (*H*).

Figure 12

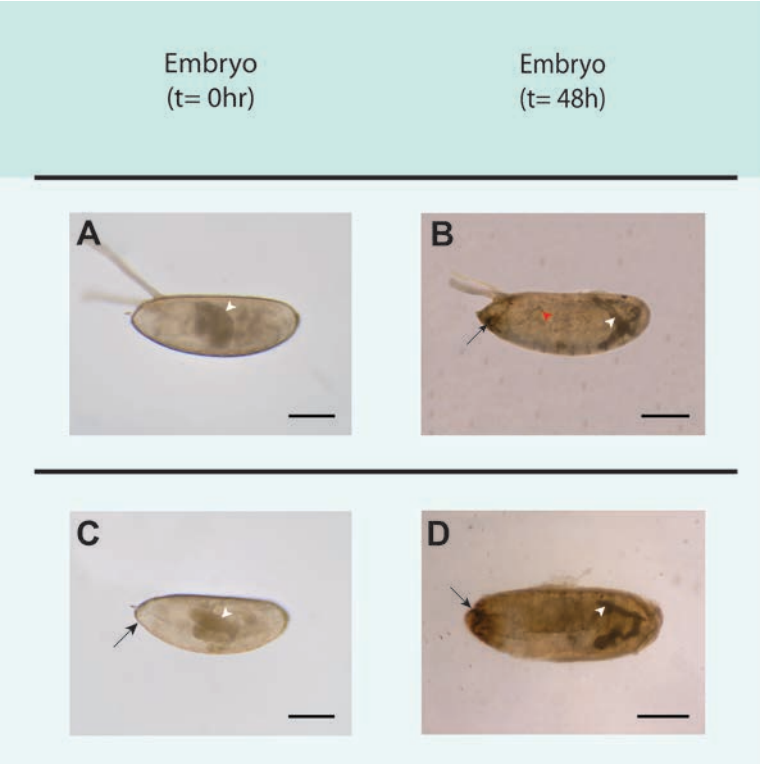

Morphology Prior and After Nanoparticle Interactions through Direct Contact-Exposure. We ask whether magnetic nanoparticles of different sizes are capable of crossing both the chorionic and vitelline membranes in the developing intact embryo. Intact embryos with both intact vitelline and chorionic membranes (A-B) and (C-D) correspond to dechorionated embryo. Intact (A) and dechorionated (C) embryos are shown before exposure to nanomaterials (t=0 hr). Corresponding dechorionated embryos are shown after exposure to nanomaterial (B-D). We use 46 nm Cop-IO-APS-CMDx-Alexa-Biotin, 76 nm Cop-IO-APS-CMDx and 40 nm Thermo-IO-APS-CMDx. Stage 15 embryos were exposed for 2 hours to nanoparticle solutions at 54mg/mL (*n=50*). Scoring using light microscopy, after 48 of recovery, revealed that IO nanoparticles seem to be capable of crossing both membranes (B-D) and tend to aggregate in the midgut and hindgut (white arrow head), tracheal system (red arrow head), the first thoracic segment, mandibular buds (md) and Malpigian tubes (mt) (black arrows), and spiracles as identified by Campos-Ortega and Hartenstein, 1985.

CHAPTER V

RESULTS: Tissue-Specific Nanomaterial Assessment:

Direct Microtransfer Interaction Route

Introduction

In order to determine which nanomaterial allowed development to proceed normally taking full advantage of the single identifiable cell nature of the *Drosophila* system small amounts of nanomaterials were microtransfered minimizing potential damage to cells caused by accelerated high pressure pulsed injections. Thus, instead of employing the well-established microinjection techniques (Kiehart, Crawford and Montague, 2007), which could prove counterproductive, microtransfering resulted in a more gentle and constant flow release of materials to the desired location with no disruption to target tissues. Developmental effects were assessed 48 hours after microdelivery in terms of overall mortality (OM) and identification of specific stage of mortality. Mortality at specific stages of development was assessed by (a) the number of embryos that failed to develop past stage 15, (b) the number of embryos that completed embryogenesis, but failed to progress to the first instar larval stage (L1), and (c) the number of larvae found dead at L1.

Preliminary Trials

Microneedle viability

In initial trials the microneedles used were prepared using a Narishige PC10 puller (Narishige USA, Inc., Greenvale, NY, USA). The Narishige PC10 puller uses a heating element and applies free fall by gravity as it's pulling force to create the fine tip of two microneedles from an original precision capillary tube of 0.4 mm. These microneedles were then beveled using a Sutter BV-10 micropipette beveler (Sutter Instruments; Novato, CA, USA). Beveling enhances the flow of solution to be injected and reduces the resistance to the microneedle penetration. Beveling is conducted by placing the tip of the microneedle over the flat, abrasive, spinning surface of a grinding plate. The microneedles obtained were not reliable because of the inconsistencies from one to another in terms of tip shape, amount of glass debris clogging the tip, and the clogging caused by the nanomaterials affinity to the microcapillary material (Fig. 9 and

Fig. 10).

The necessary pressure for unclogging the microneedle tip was in the range of 300-550 hPa and transfer values of +010 and higher (Fig. 10B). Inside an embryo, these values lead to tissue displacement and membrane rupture. Therefore, we preferred to conduct our experimentation using commercially available, highly precise microneedles as they result in consistent microtransfers as compared to laboratory-made microneedles. Moreover, we prefered a 35° angle at the microneedle's tip as more controlled microtransfer is achieved and the need for refocusing the microneedle's tip is minimized or eliminated altogether. This represents a significant advantage over other methods (Yamamoto, Sano and Hasebe, 2001).

Recovery

After being injected, the dechorionated embryos were kept under optimal conditions for recovery inside a Petri dish containing egg-laying media to assure a humid environment. Embryos were glued to the coverslip and because of that the recovery needed to take place over the cover slip. Since only one embryo was mounted on each coverslip and our usual circular coverslips are 22 mm in diameter, hatched larvae would need to crawl a vast area before reaching the egg-laying media, increasing the chances of dehydrating. For our first trials we spread a diluted mixture of dry yeast paste over the embryos to keep them hydrated and to provide a food source for the surviving individuals. This resulted in the formation of a crust over the embryos that obstruct imaging for subsequent quantification.

Recovery chamber:

For the second set of trials the recovery chamber was redesigned. To maximize the use of our materials, 4 embryos were placed inside every dish containing egg-laying media (Fig. 7A). In order to fit 4 cover slips the size of each cover slip was reduced to 5 x 5 mm. This small square was glued to 22 mm circular coverslip for microdelivery (Fig. 4C) and for visualization purposes since such a small coverslip cannot be mounted on its own in the microscope stage.

Halocarbon oil:

An extra 20 µL drop of insect saline was placed over the embryo, to maintain the necessary humidity, and the four 5 x 5 mm embryo-containing coverslips were placed surrounding a 5 x 5 mm well containing yeast paste to even the access of food for every

individual (Fig. 7A). After 48 hours the insect saline had dried, which resulted in 100% mortality. Finally, we decided to place a drop of halocarbon oil over the embryos to be injected instead of insect saline. Halocarbon oil is chemically inert, non-flammable, allows embryos to 'breathe' and offers high thermal stability and low compressibility. With this, dehydration-related mortality was eliminated.

Injection site

Microinjection is most frequently used to introduce foreign DNA into the germ cells of the embryo to generate transgenic flies (Kiehart, Crawford, and Montague, 2000). Germ cells are located in the posterior pole region, which is why most microinjection protocols suggest an entry from the posterior side of the embryo. The membrane in the posterior side is concave and presents a smaller resistance to microneedle penetration than penetration from a straight membrane perpendicular to the needle. Higher resistance to penetration is desired because the puncture can occur faster without displacing tissue. The membranes from the anterior and ventral sides are concave and the CNS is directly across it (Fig 2A). In contrast, the membrane on the dorsal side of the embryo is straight and initially we considered it an ideal entry site.

We performed two control trials to determine the optimal entry site for microinjection using physiological insect saline solutions. The trial with entry from the dorsal side required transfer values of +004 hPa while entry from the posterior side values of +008 hPa. We hypothesized that the difference is due to tissue organization and the resulting higher density of tissue found in the posterior side. After the injection trials, embryos were recovered and allowed to recuperate for 48 hours with careful consideration of temperature (25^{o}C) and humidity (70% RH). Dorsal microinjections resulted in 91% overall mortality rates compared to 44% from posterior microinjection. (Graph 1). Careful consideration of these results prompted us to continue performing our microinjections with microneedle entry site from the posterior side to diminish mortality caused by the mechanical damage of microinjection.

Determination of developmental morphological milestones

After multiple preliminary trials the following trends were chosen as scoring criteria for the quantification of mortality at specific stages of development (Fig. 11):

- *Mortality immediately after injection* (Fig. 11B, compared to untreated stage 15

embryo Fig 11A).

- *Mortality at late embryogenesis*, or mortality before L1 (stages 16 and 17) (Fig. 11D, compared to untreated stage 17 embryo Fig. 11C).
- *Mortality at L1* (Fig. 11F, compared to untreated L1 embryo Fig. 11E).
- *Survival beyond L1* (Fig. 11H, compared to untreated L3 Fig. 11G).

Volume Quantification

In order to establish the microtransfered amount of nanomaterials, the volume displacement inside the microneedle was measured every 5 injections in a preliminary trial (Table1). The length measurements were averaged from the quantifications conducted by two different individuals. The microtransfered volume was calculated as 0.00145 µL per embryo. From the initial concentrations we determined that the average amounts of implanted **IO** nanoparticles were; 1.0E-06 ng, 10 ng, 29 ng, 43 ng and 78 ng, of **Ag**; 4.3E-08 ng, 4.3E-04 ng, 4.3E-02 ng and 4.3 ng, of **Au**; 1.0E-6 ng, 1.0E-03 ng, 0.10 ng and 10 ng, of **TiO_2**; 1.0E-06 ng, 0.10 ng, 5.1 ng and 10 ng, and of **CNT**; 7.2E-10 ng, 7.2E-04 ng, 0.07 ng and 7.2 ng (Table2).

Dosage Extrapolation

We established a straightforward extrapolation based on body surface area (SA) from *Drosophila* embryos to humans. Body SA comparison for dose extrapolation is the suggested method by the US Food and Drug Administration (FDA) for clinical trials (U S Food and Drug Administration, 2005). For a *Drosophila* embryo the body SA was estimated to be 2.36×10^{-7} m^2. The SA of the embryo was then compared to the calculated SA of an average human, 1.74 m^2. Using a conversion factor between embryo SA and human SA, the equivalent microtransfered volume was calculated as 10.7 mL, which represents only 0.018% of the volume of an average human. In addition the dosage from each original concentration was calculated in $\mu g/m^2$ (Table 2).

Data Distribution Analysis

In order to establish what statistical analyses were going to be conducted, data distribution had to be assessed first. The data obtained consists of discrete values and the 3

mortality scoring criteria were set as 1, 2 and 3 for quantification purposes. In order to determine if the data sets followed a normal distribution a Shapiro–Wilk test was conducted considering 0.05 as our statistical level of significance (α). This test tests the null hypothesis that a sample came from a normally distributed population (data set). Since some of our data sets present a $W < 0.05$, rejecting the null hypothesis, it was concluded that they do not preset a normal distribution. Having a mixture of normal and non-normal distributed data sets (W{0.00000, 0.9998}) conducting parametric analysis could add an error to the analysis. Therefore, we decided to conduct a non-parameteric analysis.

Non-Parametric Analysis

Most non-parametric analyses require binomial data were for each observation i, the response Yi can take only two values coded 0 and 1. For this reason, we decided to regroup our data. Overall mortality is the sum of our 3 scoring criteria (mortality after injection, mortality before L1 and mortality at L1) against the number of individuals that survived beyond L1 ((3 scoring criteria) – 50). With our data rearranged we conducted a Fischer's exact test. Fischer's test allows us to determine if 2 binary proportions (categorical data) are equal or different when our samples are independent. We compared control trials against each other, and the experimental trials against their corresponding control. The resulting p-values can be found on Tables 3, 4, and 5.

Control trials

Overall mortality

When assessing mortality it was necessary to establish how much of it was contributed by sample mishandling (Graph 2). Since the embryos needed to be dechorionated in order to be injected, we quantified mortality rates after dechorionation and subsequent 48h of recovery to mimic the handling process. Mortality rates were also established after injection of insect saline solution. This was done to establish the mortality contributed by the mechanical damage caused by the puncturing when microinjecting. The nanomaterials employed were in a solution of H_2O or BSA 10% so we also quantified mortality rates after injection with H_2O and BSA 10% separately.

These analyses were done two ways: comparing the data of injections with insect saline,

H_2O and BSA 10% against the data of dechorionated embryos, and comparing the data of injections with H_2O and BSA 10% against insect saline. After 48 hours of recovery in the dechorionation trial 62% of the individuals survived (38% OM), compared to the 56% of embryos injected with insect saline (44%OM), 48% of embryos injected with H_2O (52%OM) and 46% of embryos injected with BSA 10% (54% OM) (Graph 2). In every case the Fischer's p-value was greater than 0.05. P-values ranging from 0.16 to 1.0 indicate no statistical difference between the data sets. We found that there are no statistically relevant differences in mortality rates (or survival) between injecting insect saline and simply removing the chorion membrane (P = 0.685). This assures us that, statistically speaking, the mechanical damage of injection does not lead to a significant increase in mortality. Results also suggest that there is no significant difference between mortality rates of embryos injected with H_2O and BSA (P = 1).

Mortality at different stages of development

All of the control groups have their highest mortality in late embryogenesis (mortality before L1) (Graph 2).

Iron Oxide Nanoparticles

Overall mortality

IO nanoparticles were suspended in H2O so Fischer's test was used to compare the different treatments against the H2O trials.

Cop-IO-APS-Alexa-Biotin nanoparticles rejected the null hypothesis at all but the two lowest concentrations of microinjected nanomaterial when compared to H_2O. An OM of 54% when treated with the initial concentration of 7.0E-07 µg/µL and an OM of 64% when treated with the second lowest concentration of 7.0 µg/µL, and p-values of 1 and 0.31, suggests a statistical similarity between the OM in this treatment and the control (Graph 3). Treatment with Cop-IO-APS-Alexa-Biotin nanoparticles at concentrations of 20 µg/µL, 30 µg/µL, and 54 µg/µL lead to higher OM values of 76%, 92%, and 96%. The increased difference between the treatments and the control represent a statistically relevant increased toxic effect at the 3 highest concentrations (p =0.021-0) (Graph 3).

Cop-IO-APS-CMDx nanoparticles rejected the null hypothesis at the two highest

concentrations of microinjected nanomaterial when compared to H_2O. We obtained OM values of 52%, 56%, and 72% when treated with concentration of 7.0E-07 µg/µL, 7.0 µg/µL, and 20 µg/µL, and p-values of 1, 0.84, and 0.063. The results after treating with the 3 lowest concentrations suggest a statistical similarity between the OM of the treatment and the control (Graph 4). On the other hand, treatment with Cop-IO-APS-CMDx nanoparticles at concentrations of 30 µg/µL and 54 µg/µL lead to OM values of 74% and 94%. The increased difference between the treatments and the control represent a statistically relevant increased toxic effect at the 2 highest concentrations (p =0.038-0) (Graph 4).

Treatment with Thermo-IO-CMDx nanoparticles show similar results to that of Cop-IO-APS-CMDx. Thermo-IO-CMDx nanoparticles also rejected the null hypothesis at the two highest concentrations of microinjected nanomaterial when compared to H_2O. We obtained OM values of 52%, 52%, and 72% when treated with concentration of 7.0E-07 µg/µL, 7.0 µg/µL and, 20 µg/µL, and p-values of 1 and 0.063. These results suggest a statistical similarity between the OM of the treatment and the control when treating with the 3 lowest concentrations (Graph 5). In the treatment with the 2 highest concentrations of Thermo-IO-CMDx nanoparticles, 30 µg/µL and 54 µg/µL, OM values increase to 90% and 98%. Just as with the treatment with Cop-IO-APS-CMDx, there is a statistically relevant increased toxic effect at the 2 highest concentrations (p =0) (Graph 5).

Mortality at different stages of development

Treatment with Cop-IO-APS-Alexa-Biotin nanoparticles leads to the highest mortality percentage at late embryogenesis with the 2 lowest concentrations, and immediately after microinjection with the 3 highest concentrations (Graph 3). On the other hand, Cop-IO-APS-CMDx and Thermo IO-CMDx nanoparticles show higher mortality with the 3 lowest concentrations at late embryogenesis, but with the 2 highest concentrations the highest mortality occurs after microinjection (Graphs 4-5).

Silver, gold, titanium dioxide, single-wall carbon nanotubes, and multi-wall carbon nanotubes

Overall mortality

Ag nanoparticles, Au nanoparticles, TiO_2 nanoparticles, SWCNT, and MWCNT were

suspended in BSA 10% so Fischer's test was used to compare the different treatments against the BSA 10% trials.

Ag nanoparticles rejected the null hypothesis at all but the lowest concentrations of microinjected nanomaterial when compared to BSA 10%. An OM of 62% when treated with the initial concentration of 3.0E-08 µg/µL and a p-value of 0.544, suggests a statistical similarity between the OM in this treatment and the control (Graph 6). Treatment with Ag nanoparticles at concentrations of 3.0E-04 µg/µL, 0.03 µg/µL, and 3.0 µg/µL lead to higher OM values of 86%, 90%, and 92%. The increased difference between the treatments and the control represent a statistically relevant increased toxic effect at the 3 highest concentrations (p =0.001-0) (Graph 6).

Au nanoparticles rejected the null hypothesis at the 2nd highest and highest concentrations of microinjected nanomaterial when compared to BSA 10%. Au nanoparticles show an OM of 64% and 72% when treated at concentrations of 7.0E-07µg/µL and 7.0E-04µg/µL, and p-values of 0.416- 0.097 suggesting a statistical similarity between these treatments and the control (Graph 7). Treatment with Au nanoparticles at concentrations of 0.07 µg/µL and 7.0 µg/µL leads to higher OM values of 80%, and 88%. The increased difference between the treatments and the control represent a statistically relevant increased toxic effect at the 2 highest concentrations (p =0.01-0) (Graph 7).

TiO_2 nanoparticles rejected the null hypothesis in all but the lowest concentration of microinjected nanomaterial when compared to BSA 10%. An OM of 66% when treated with the initial concentration of 7.0E-07 µg/µL and a p-value of 0.307, suggests a statistical similarity between the OM in this treatment and the control (Graph 8). Treatment with TiO_2 nanoparticles at concentrations of 0.07 µg/µL, 3.5 µg/µL, and 7.0 µg/µL lead to higher OM values of 76%, 82%, and 86%. The increased difference between the treatments and the control represent a statistically relevant increased toxic effect at the 3 highest concentrations (p =0.005-0.001) (Graph 8).

SWCNT rejected the null hypothesis at all but the lowest concentrations of microinjected nanomaterial when compared to BSA 10%. An OM of 62% when treated with the initial concentration of 5.0E-10 µg/µL and a p-value of 0.544, suggests a statistical similarity between the OM in this treatment and the control (Graph 9). Treatment with SWCNT at concentrations of

5.0E-04 µg/µL, 0.05 µg/µL, and 5.0 µg/µL lead to higher OM values of 82%, 82%, and 84%. The increased difference between the treatments and the control represent a statistically relevant increased toxic effect at the 3 highest concentrations (p=0.005-0.002) (Graph 9).

Although treated at the same amounts, SWCNT and MWCNT lead to different results. Treatment with MWCNT at the concentrations of 5.0E-10 µg/µL, and 5.0 µg/µL lead to higher OM values of 76%, and 78%. The increased difference between the treatments and the control represent a statistically relevant increased toxic effect at the lowest and highest concentrations (p=0.035-0.02) (Graph 10). MWCNT at concentrations of 5.0E-04 µg/µL, and 0.05 µg/µL lead to OM of 72% and 74% and p-values of 0.097 and 0.06, suggest a statistical similarity between the OM in these treatments and the control (Graph 10).

Mortality at different stages of development

Treatment with Ag nanoparticles leads to the highest mortality percentage with the lowest concentration at late embryogenesis, but with the other 3 concentrations the highest mortality occurs after microinjection (Graph 6). Treatment with Au nanoparticles leads to higher mortality with the lowest concentration at late embryogenesis, with the intermediate concentrations (7.0E-04 µg/µL and 0.07 µg/µL) at L1, and with the highest concentration after injection and at L1 (Graphs 7). Treatment with TiO_2 nanoparticles leads to higher mortality percentages with the lowest concentration at late embryogenesis, with the intermediate concentrations at L1, and with the highest concentration after injection (Graphs 8).

Treatment with SWCNT leads to higher mortality percentages with concentrations from the lowest to the 2nd highest at late embryogenesis, and with the highest concentration at L1 (Graph 9). On the other hand, treatment with MWCNT leads to higher mortality percentages with the lowest concentration at late embryogenesis, with the second lowest after injection and at late embryogenesis, and with the 2 highest it shifts back to occurring at late embryogenesis (Graph 10).

CHAPTER VI

RESULTS: Passive Transport Nanomaterial Assessment:

Direct Contact-Exposure Route

Introduction

Nanoparticles' capacity to cross complex biological membranes is an important aspect that deserves further study as these nanomaterials may hold promise as drug delivery platforms (nanocarriers) and the *Drosophila* system is suitable for their study. Furthermore, the direct-contact exposure route can be employed to model environmental exposure. In order to determine which nanomaterial are capable of crossing the membranes of a developing embryo we exposed stage 15 embryos to nanomaterial solution for 3 hours.

Preliminary Trials

Bioacummulation capabilities

Initially we also try assessing nanomaterials bioacummulation capability using light microscopy. We exposed stage 15 embryos to nanomaterial solution for 2 hours and allow the embryos to recover for 48 hours. Observation using light microscopy suggest that IO-nanoparticles are all capable of crossing both chorionic and vitelline membranes (Fig. 12B-D) and tend to aggregate in the midgut, hindgut, tracheal system, the first thoracic segment, mandibular buds (md), malpigian tubes (mt), and spiracles as identified by Campos-Ortega and Hartenstein, 1985. This was a qualitative assessment and because 48 hours had passed some embryos had died and others had hatched. The dead embryos could not be recovered for ICP-MS analysis because they were too fragile. Henceforth, we opted for preparing the samples for ICP-MS after 3 hours of contact with nanomaterial solution without allowing the embryos to recover for 48 hours.

Inductively Coupled Plasma Mass Spectrometry Analysis

Pace Analytical conducted our ICP-MS analysis. The equipment detection limit for Fe is 5,000 ppb, and for Au, Ag, and Ti is 50.0 ppb. We conducted a control experiment in which we try detecting Fe, Ag, Au, and Ti in 2 groups with chorion membrane and 2 without chorion (n = 50 each). The equipment was not able to detect these metal traces (Table 6). The materials

involved in solution and sample preparation were not detected either (Table 7). Nanomaterials were tested at 2 different concentrations and the lowest concentration was the PEC. The equipment was not able to detect these metal traces in any of the groups treated with IO nanoparticles (Table 8). In groups treated with Ag, Au, and Ti the equipment only detected those metals in the groups of embryos with their intact membrane (Table 9). This suggests that with 3 hours of incubation Ag, Au and TiO_2 nanoparticles do not attach to the vitelline membrane and are not transported across the vitelline membrane, or that the nanomaterials transported across the vitelline membrane were in quantities under the detection limit of the equipment.

CHAPTER VII

TABLES AND GRAPHS

Tables

Length	Averaged Length (µL)	Displaced Length (µL)	Volume (μm_3)	Volume (µL)
X_i	579.093750			
X_5	587.903200	8.809450	6918925.851445	0.006919
X_{10}	595.078250	7.175050	5635271.093021	0.005635
X_{15}	603.237150	8.158900	6407985.076180	0.006408
X_{20}	612.704300	9.467150	7435482.223579	0.007435
X_{25}	625.095150	12.390850	9731750.834204	0.009732

Table 1. Microtransfered volume quantification.

Nanomaterial	Initial Concentration (µg/µL)	Nanomaterials per Embryo (ng)	Nanomaterials per Human (µg)	Dosage (µg/ m^2)
IO	7.00E-07	1.0E-06	0.0075	4.3E-03
	7	10	7.5E+04	4.3E+04
	20	29	2.1E+05	1.2E+05
	30	43	3.2E+05	1.8E+05
	54	78	5.8E+05	3.3E+05
Ag	3.0E-08	4.3E-08	0.0075	4.3E-03
	3.0E-04	4.3E-04	7.5E+02	4.3E+02
	0.03	4.3E-02	3.7E+04	2.2E+04
	3	4.3	7.5E+04	4.3E+04
Au	7.0E-07	1.0E-06	3.2E-04	1.8E-04
	7.0E-04	1.0E-03	3.2	1.8
	0.07	0.1	3.2E+02	1.8E+02
	7	10	3.2E+04	1.8E+04
TiO2	7.0E-07	1.0E-06	5.3E-06	3.1E-06
	0.07	0.1	5.3	3.1
	3.5	5.1	5.3E+02	3.1E+02
	7	10	5.3E+04	3.1E+04
CNT	5.0E-10	7.2E-10	7.5E-03	4.3E-03
	5.0E-04	7.2E-04	7.5	4.3
	0.05	0.07	7.5E+02	4.3E+02
	5	7.2	7.5E+04	4.3E+04

Table 2. Microtransfered nanomaterial amounts and dosage quantification.

Comparison				
Treatment 1	**vs**	**Treatment 2**	**Fischer's p-value**	**Null hypothesis**
Dechorionation	vs	Insect Sline	0.685	agrees
		H2O	0.228	
		BSA 10%	0.16	
Insect Saline		H2O	0.548	
		BSA 10%	0.424	
H2O		BSA 10%	1	

Table 3. Statistical comparison of control groups through Fisher's exact test for unpaired samples.

Comparison					
Treatment 1	**vs**	**Treatment 2**		**Fischer's p-value**	**Null hypothesis**
H2O	vs	Cop-IO-APS-Alexa-Biotin	7E-07	1	agrees
			7	0.3111	
			20	0.021	rejects
			30	0	
			54	0	
		Cop-IO-APS-CMDx	7E-07	1	agrees
			7	0.8411	
			20	0.063	
			30	0.038	rejects
			54	0	
		Thermo-IO-CMDx	7E-07	1	agrees
			7	1	
			20	0.063	
			30	0	rejects
			54	0	

Table 4. Statistical comparison of H_2O vs IO-nanoparticle treatment through Fisher's exact test for unpaired samples.

Comparison					
Treatment 1	**vs**	**Treatment 2**		**Fischer's p-value**	**Null hypothesis**
BSA 10%	vs	Ag	3E-08	0.544	agrees
			3E-04	0.001	rejects
			0.03	0	
			3	0	
		Au	7E-07	0.42	agrees
			7E-04	0.097	
			0.07	0.01	rejects
			7	0	
		TiO2	7.00E-07	0.307	agrees
			0.00	0.035	rejects
			0.1	0.005	
			7	0.001	
		SWCNT	5E-10	0.544	agrees
			5E-04	0.005	rejects
			0.05	0.005	
			5	0.002	
		MWCNT	5E-10	0.035	rejects
			5E-04	0.097	agrees
			0.05	0.06	
			5	0.02	rejects

Table 5. Statistical comparison of BSA 10% vs nanomaterial treatment through Fisher's exact test for unpaired samples.

Treatment	Chorion	Measurement (ppb)
Blank	W/O	ND
		ND
	W	ND
		ND

Table 6. ICP-MS Analysis of *Drosophila* embryos without nanomaterial treatment. (W = with, W/O = without) (n = 50).

Treatment	Content	Measurement (ppb)
H2O	10µL H2O	ND
Agar	0.01 g agar	ND
Insect Saline	10µL IS	ND
BSA 10%	10µL BSA 10%	ND
Cop-IO-APS-Alexa-Biotin	10µL at 7µg/µL	7190
Cop-IO-APS-CMDx	10µL at 7µg/µL	13100
Thermo-IO-CMDx	10µL at 7µg/µL	24400
Ag	10µL at 3µg/µL	56700
Au	10µL at 7µg/µL	662
TIO2	10µL at 7µg/µL	112000

Table 7. ICP-MS Analysis of materials involved in solutions or sample preparation. (n = 50).

Treatment	Concentration (µg/µL)	Chorion	Measurement (ppb)
Cop-IO-APS- Alexa-Biotin	7.00E-07	W/O	ND
			ND
		W	ND
			ND
	7	W/O	ND
			ND
		W	ND
			ND
Cop-IO-APS-CMDx	7.00E-07	W/O	ND
			ND
		W	ND
			ND
	7	W/O	ND
			ND
		W	ND
			ND
Thermo-IO-CMDx	7.00E-07	W/O	ND
			ND
		W	ND
			ND
	7	W/O	ND
			ND
		W	ND
			ND

Table 8. ICP-MS Analysis of *Drosophila* embryos subjected to IO-nanoparticle treatment. (W = with, W/O = without) (n = 50).

Treatment	Concentration (µg/µL)	Chorion	Measurement (ppb)
Ag	3.00E-08	W/O	ND
			ND
		W	ND
			ND
	3	W/O	ND
			ND
		W	820
			840
Au	7.00E-07	W/O	ND
			ND
		W	ND
			ND
	7	W/O	ND
			ND
		W	1260
			954
TiO2	7.00E-07	W/O	ND
			ND
		W	ND
			ND
	7	W/O	ND
			ND
		W	710
			908

Table 9. ICP-MS Analysis of *Drosophila* embryos subjected to silver, gold, and titanium dioxide nanoparticle treatment. (W = with, W/O = without) (n = 50).

Graphs

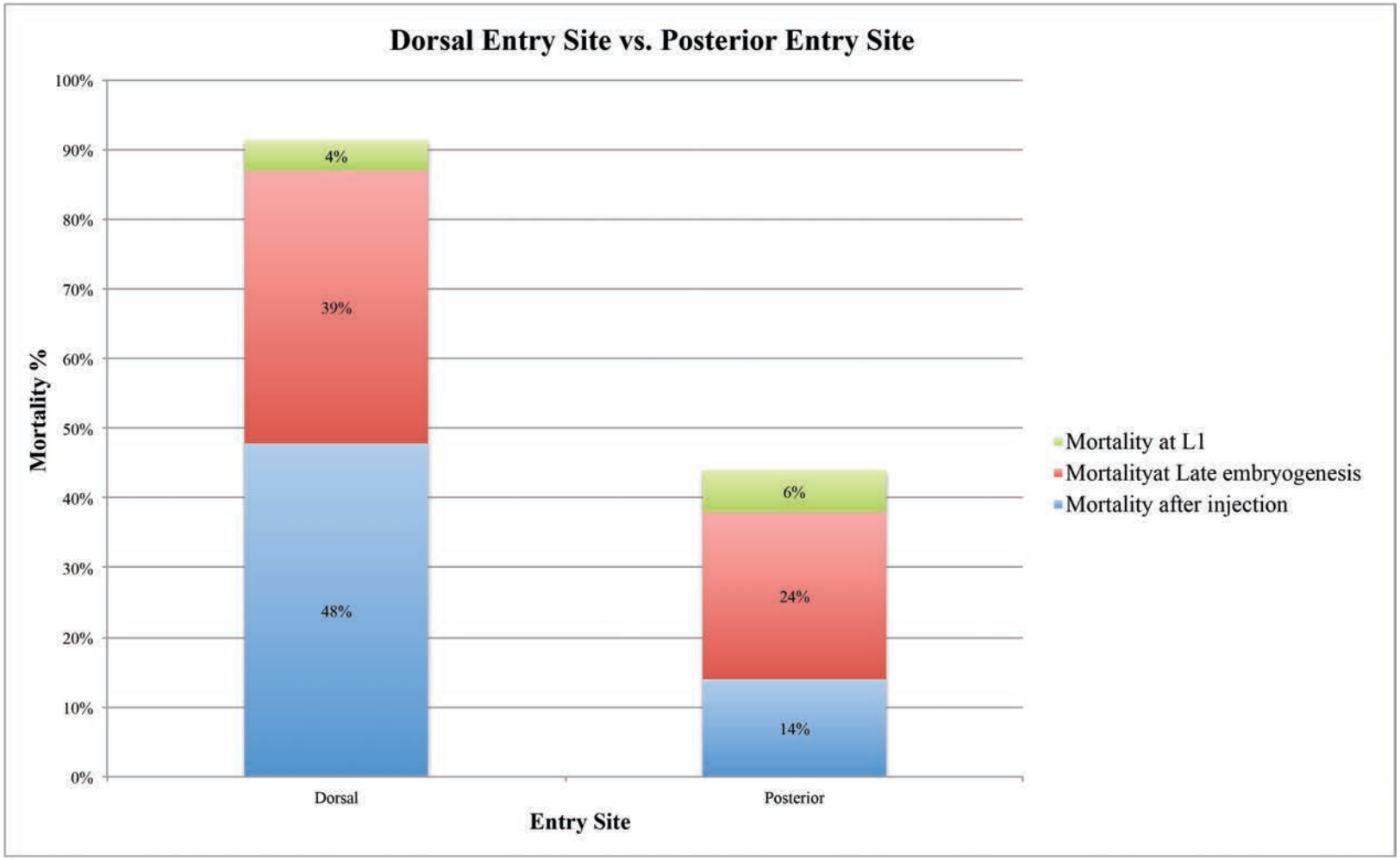

Graph 1. Mortality comparison of embryos injected with dorsal entry site (n=23) and posterior entry site (n=50), with insect saline.

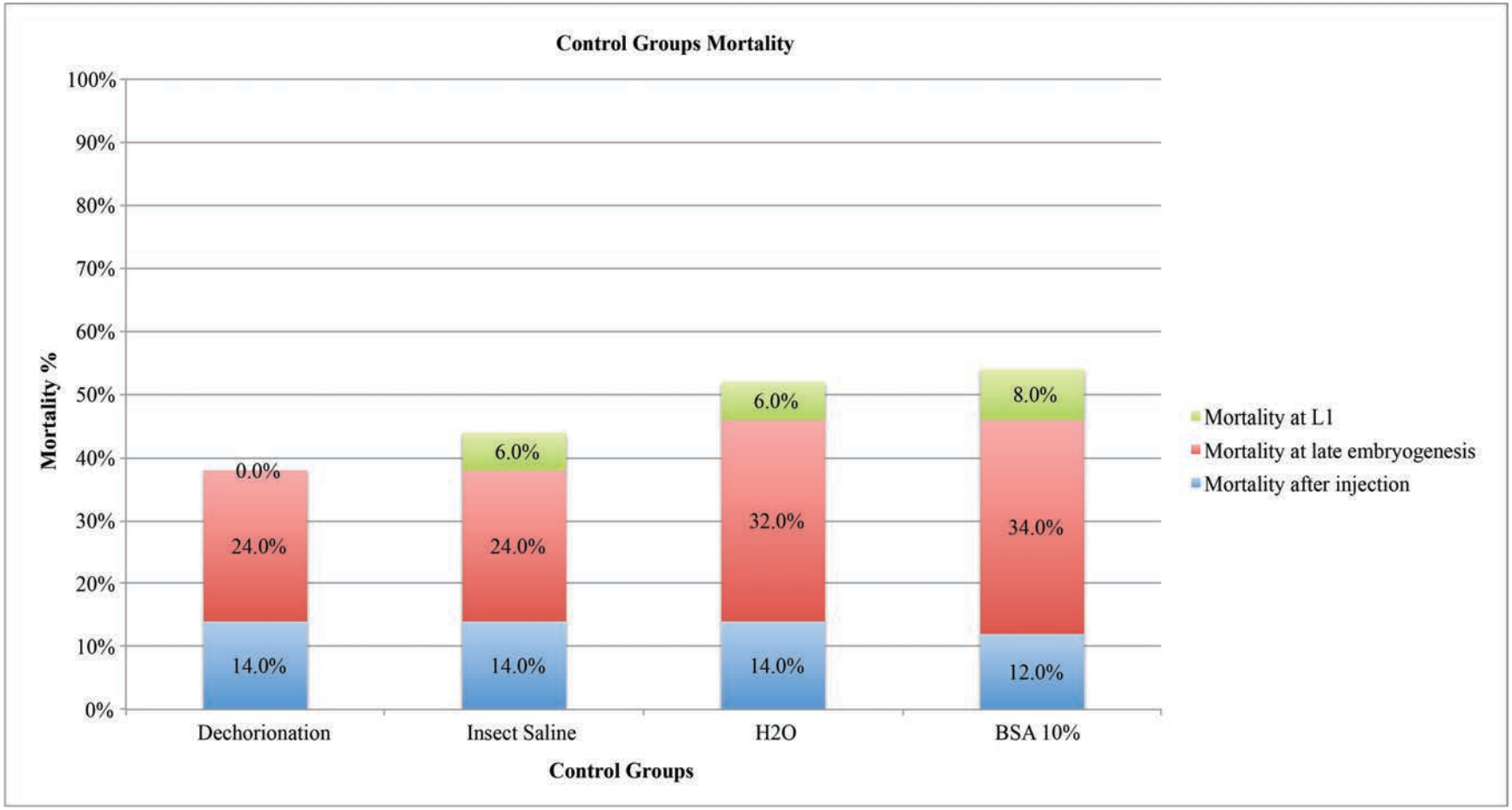

Graph 2. Mortality comparison of embryos only subjected to the removal of the chorion membrane (dechorionation), embryos injected with insect saline solution, embryos injected with H_2O, and embryos injected with BSA 10% (n=50).

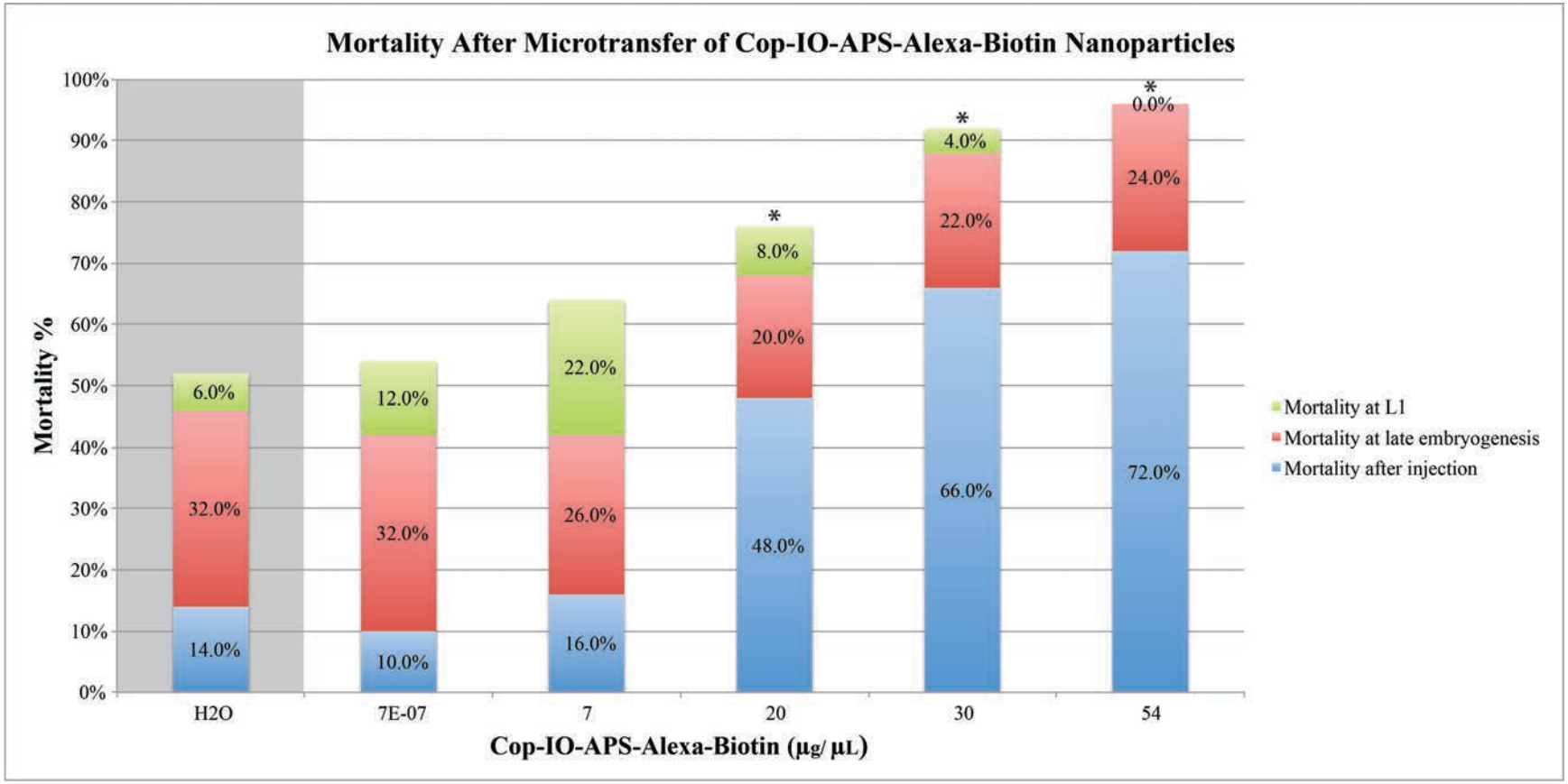

Graph 3. Mortality comparison of embryos injected with Cop-IO-APS-Alexa-Biotin nanoparticles and embryos injected with H_2O (n=50).

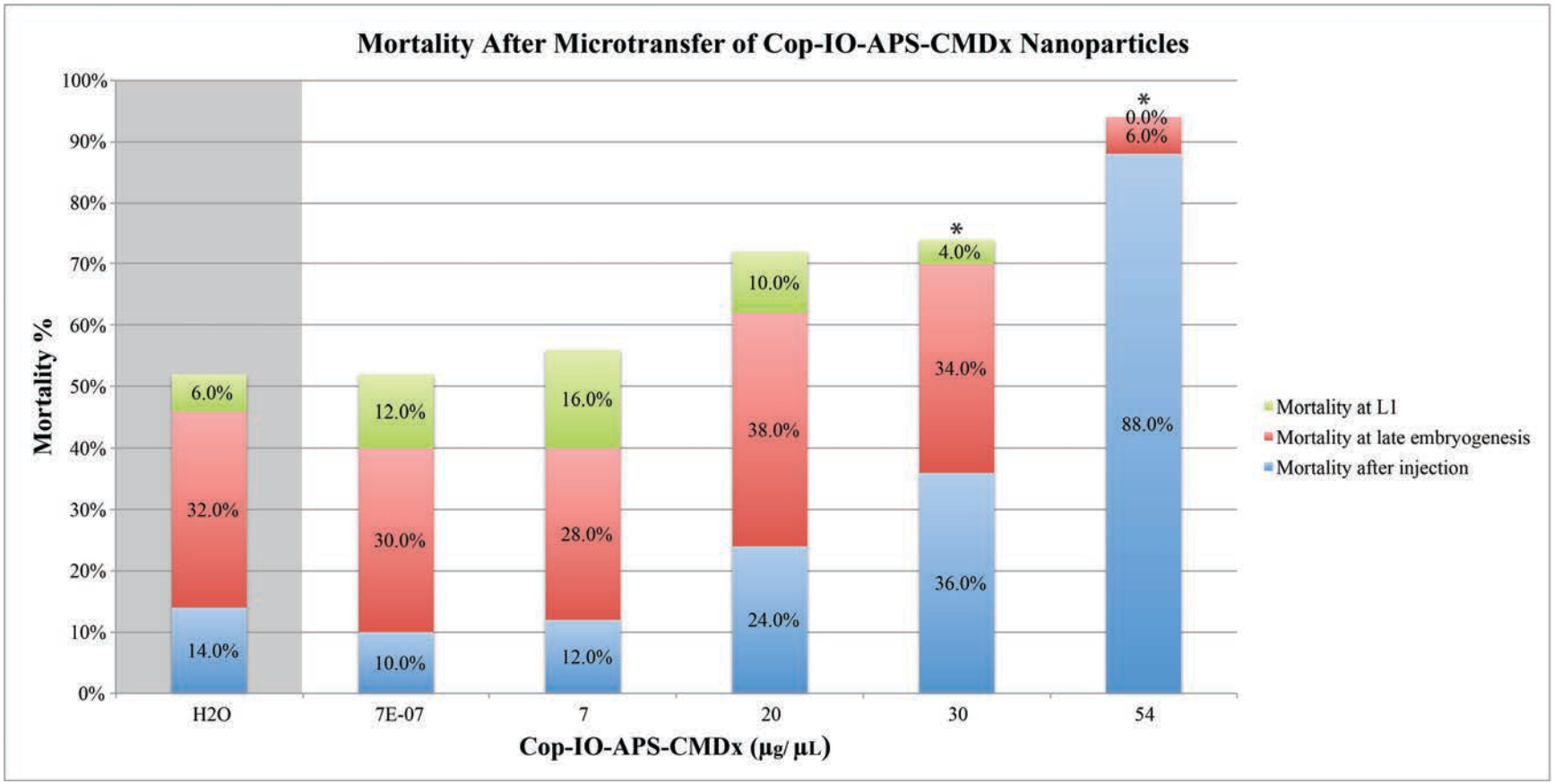

Graph 4. Mortality comparison of embryos injected with Cop-IO-APS-CMDx nanoparticles and embryos injected with H_2O (n=50).

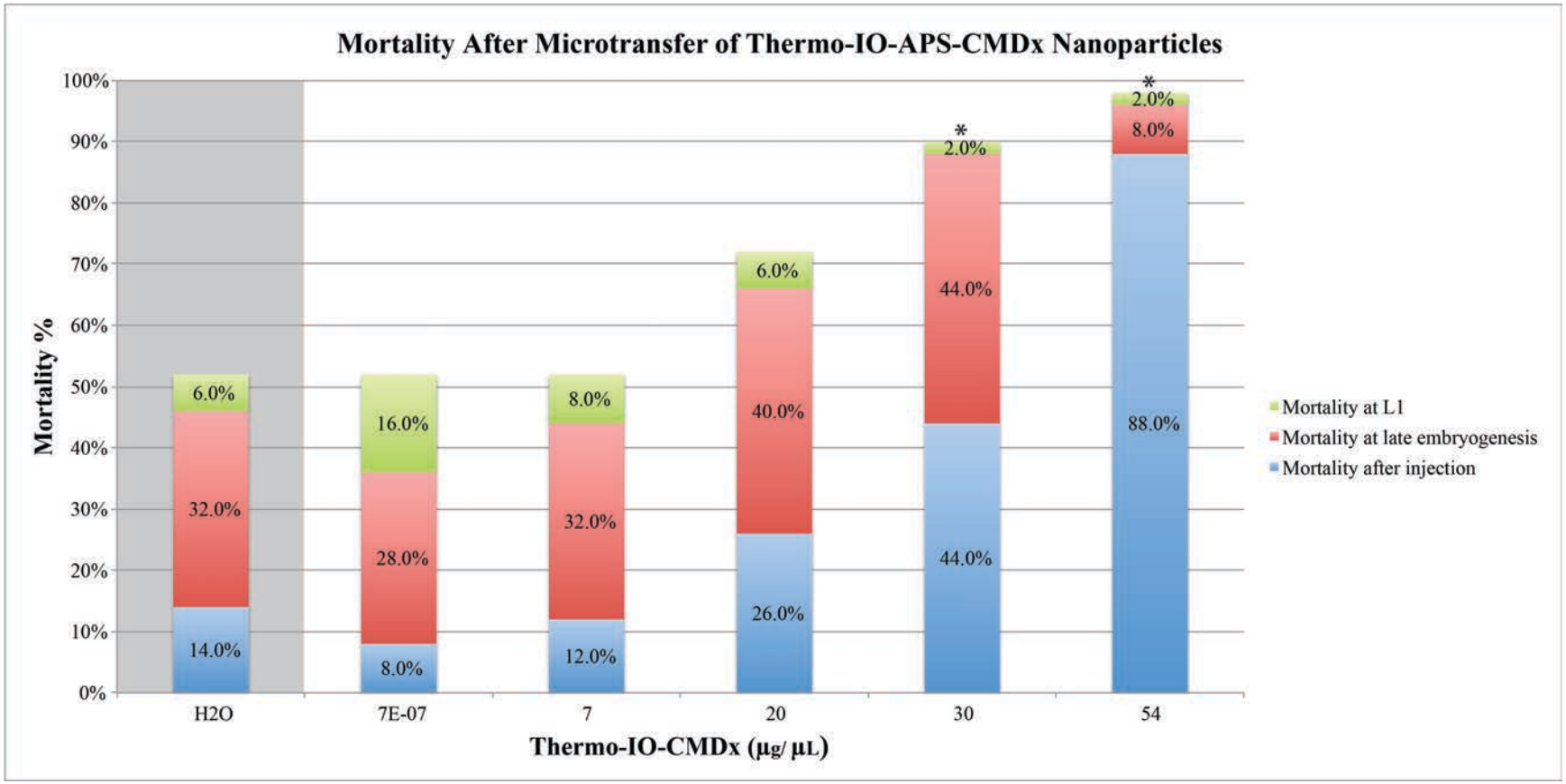

Graph 5. Mortality comparison of embryos injected with Thermo-IO-CMDx nanoparticles and embryos injected with H_2O (n=50).

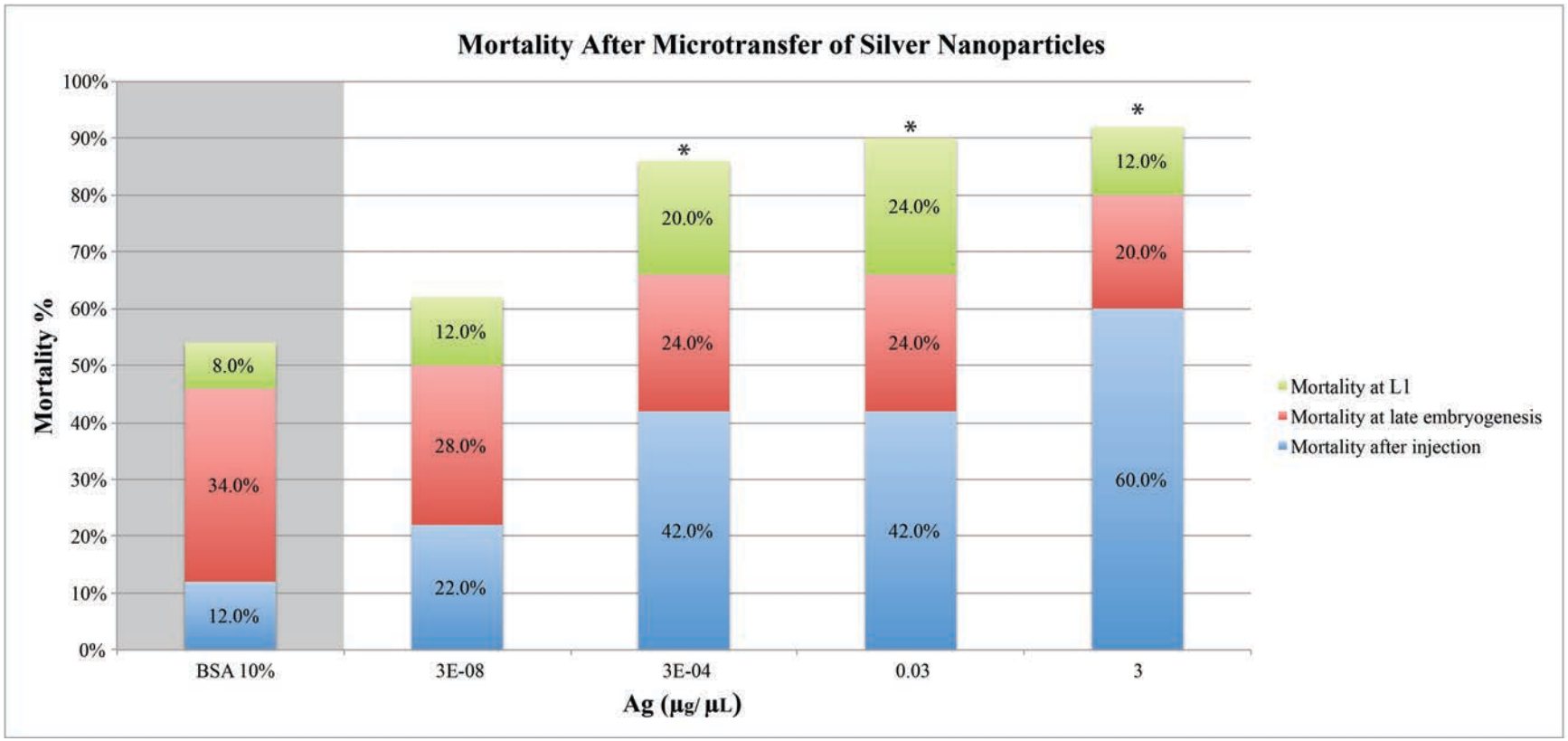

Graph 6. Mortality comparison of embryos injected with Silver (Ag) nanoparticles and embryos injected with BSA 10% (n=50).

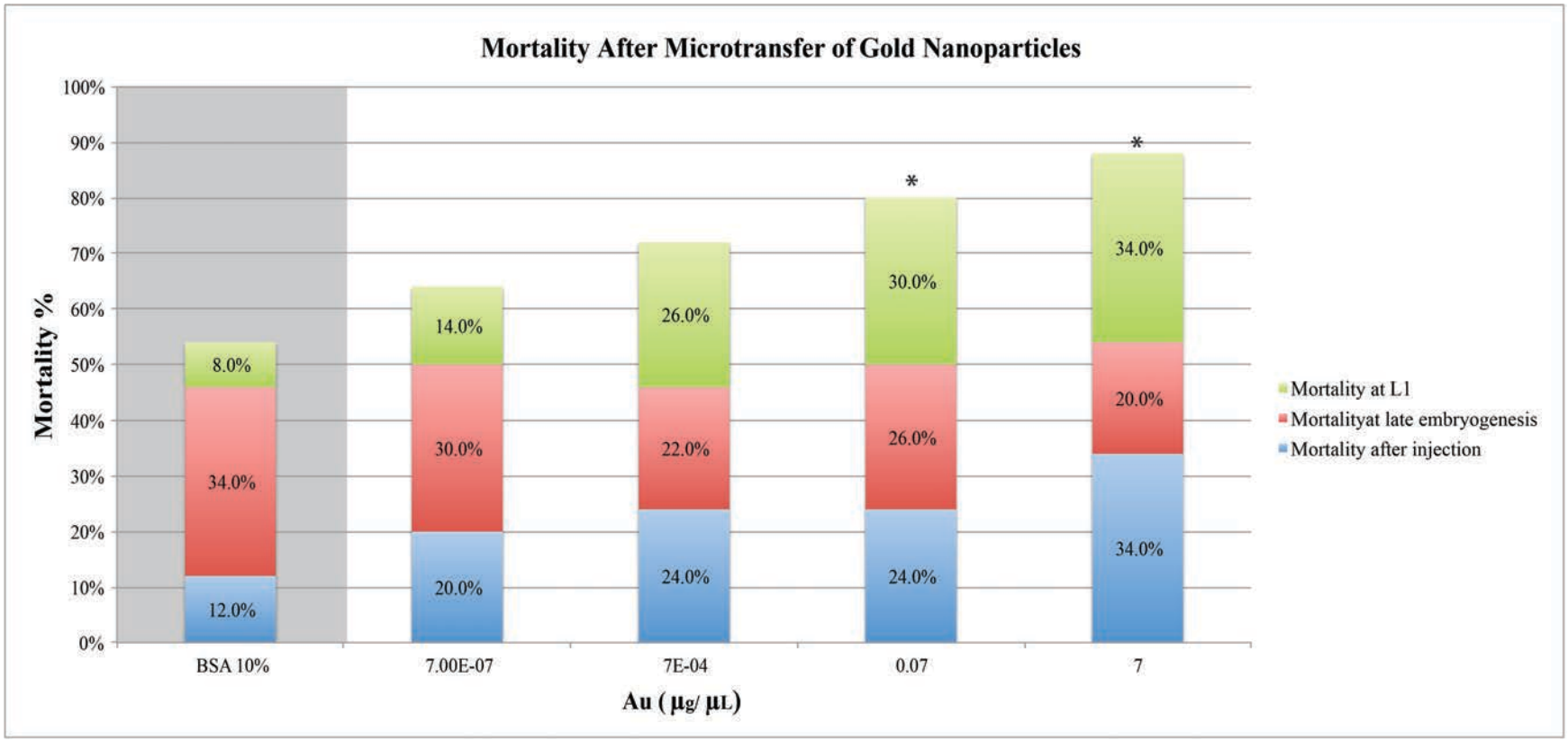

Graph 7. Mortality comparison of embryos injected with Gold (Au) and embryos injected with BSA 10% (n=50).

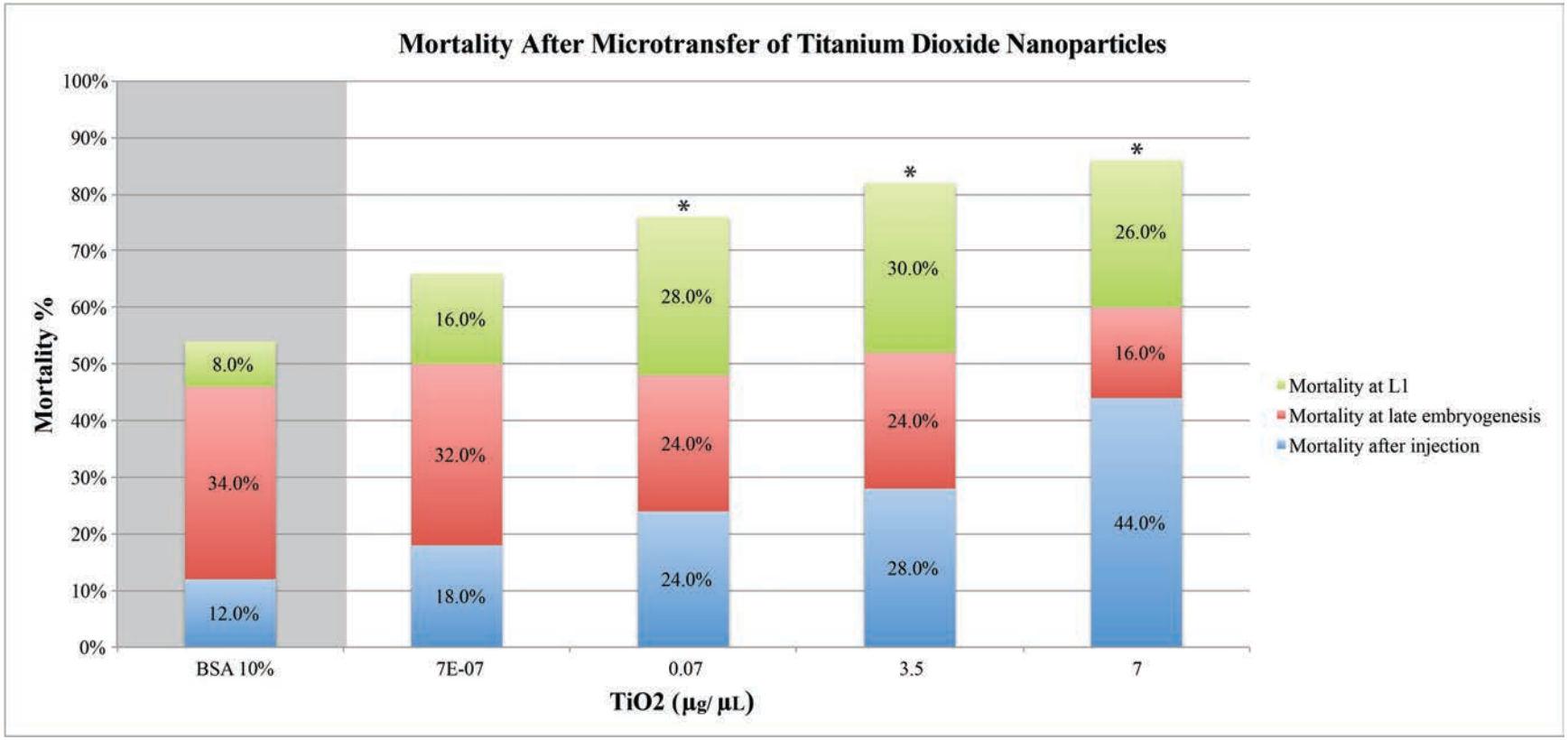

Graph 8. Mortality comparison of embryos injected with Titanium dioxide (TiO_2) and embryos injected with BSA 10% (n=50).

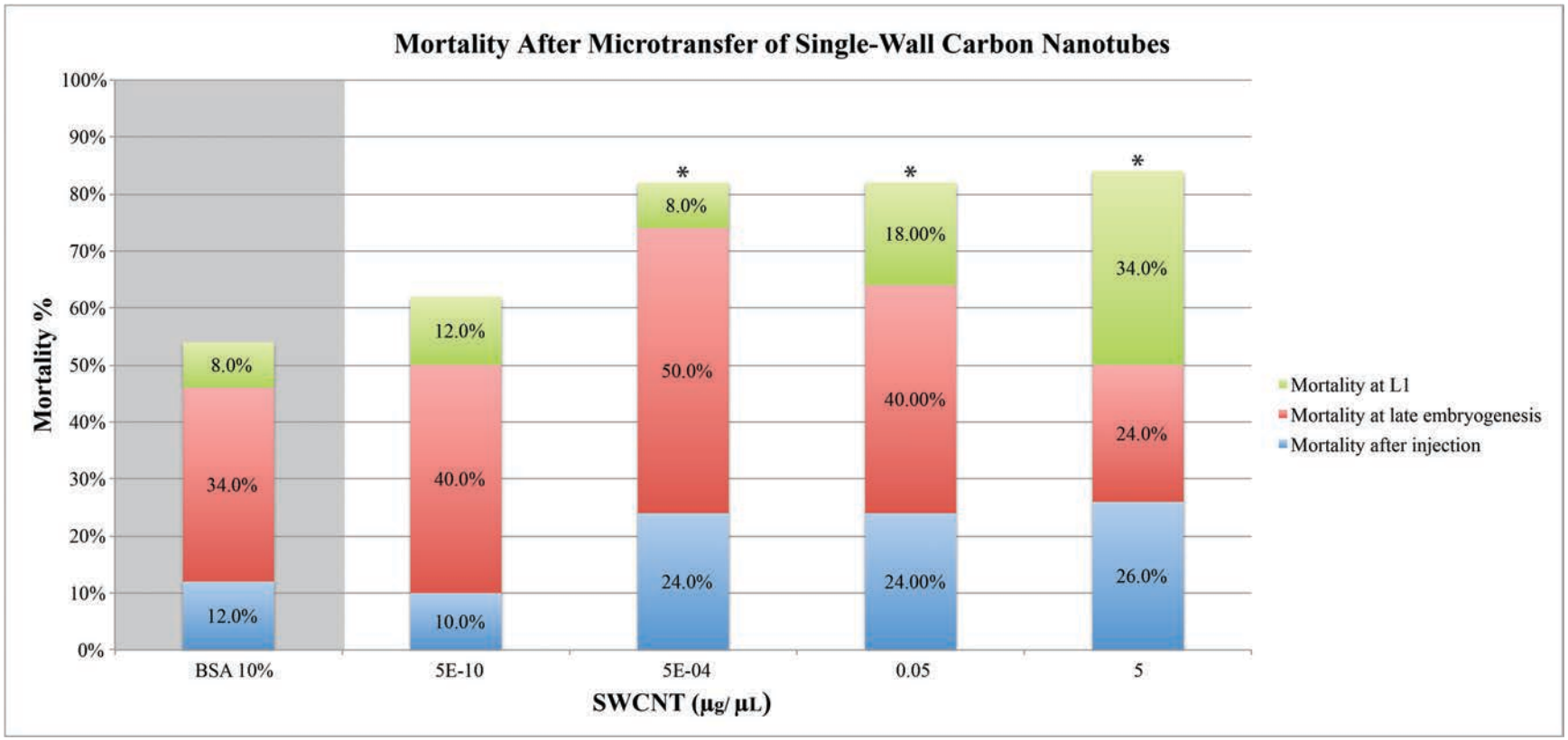

Graph 9. Mortality comparison of embryos injected with Single-wall Carbon Nanotubes (SWCNT) and embryos injected with BSA 10% (n=50).

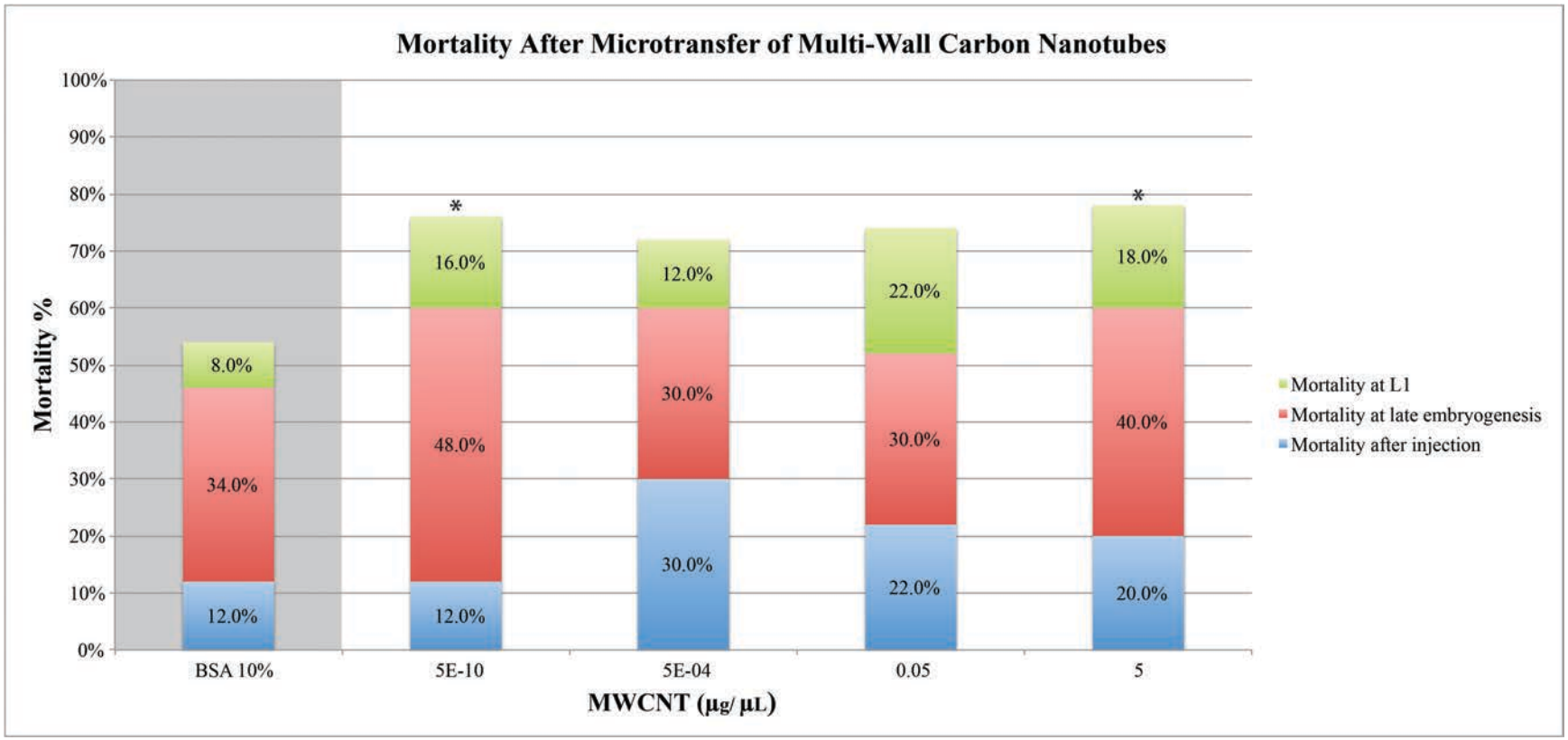

Graph 10. Mortality comparison of embryos injected with Multi-wall Carbon Nanotubes (MWCNT) and embryos injected with BSA 10% (n=50).

CHAPTER VIII

DISCUSSION

Tissue-Specific Nanomaterial Assessment

Iron Oxide Nanoparticles

The 3 highest concentrations of Cop-IO-APS-Alexa-Biotin nanoparticles have statistically relevant effects in *Drosophila* embryo viability. Furthermore, treatment with Cop-IO-APS-Alexa-Biotin nanoparticles shows a shift in scoring criteria with highest mortality from late embryogenesis to immediately after injection, from the 2nd to the 3rd concentration. This shift suggests that embryos die faster after an increase from 7 µg/µL to 20 µg/µL.

The 2 highest concentrations of Cop-IO-APS-CMDx nanoparticles have statistically relevant effects in *Drosophila* embryo viability. In the case of Cop-IO-APS-CMDx nanoparticles treatment, the shift in scoring criteria with highest mortality from late embryogenesis to immediately after injection occurs from the 3rd to the 4th concentration (20 µg/µL to 30 µg/µL). This suggests that the biocompatibility and stabilizing properties of CMDx are having a favorable effect in delaying the toxic effect to higher concentrations.

As with Cop-IO-APS-CMDx nanoparticles, Thermo-IO-CMDx treatment presents statistically relevant effects in *Drosophila* embryo viability only at the 2 highest concentrations. Even though the 2 highest concentrations of Thermo-IO-CMDx present higher overall mortality than the 2 highest concentrations of Cop-IO-APS-CMDx, the shift on highest mortality from late embryogenesis to immediately after injection occurs from the 4th to the 5th concentration (30 µg/µL to 54 µg/µL). This suggests that nanoparticles synthesized by thermo-decomposition lead to higher overall mortality, but nanoparticles synthesized be co-precipitation present a more acute effect since the individuals die faster at lower concentrations.

Silver Nanoparticles

All but the PEC of Ag nanoparticles present a statistically relevant effects in *Drosophila* embryo viability. Furthermore, treatment with Ag nanoparticles shows a shift in scoring criteria with highest mortality from late embryogenesis to immediately after injection, from the 1st (PEC) to the 2nd concentration (3.0E-08 µg/µL to 3.0E-04 µg/µL). This suggests that treatment with Ag nanoparticles elicit an acute toxic effect and that Ag nanoparticles have a low effective dose.

Gold Nanoparticles

The 2 highest concentrations of Au nanoparticles have statistically relevant effects in *Drosophila* embryo viability. Also, treatment with Au nanoparticles shows a shift in scoring criteria with highest mortality from late embryogenesis to L1 and then to immediately after injection.

Titanium Dioxide Nanoparticles

The 3 highest concentrations of TiO_2 nanoparticles have statistically relevant effects in *Drosophila* embryo viability. As with treatment with Au nanoparticles, TiO_2 nanoparticles show a shift in scoring criteria with highest mortality from late embryogenesis to L1 and then to immediately after injection. Therefore, since TiO_2 and Au nanoparticles were administered at the same concentrations, TiO_2 elicit a more acute toxic effect and have a lower effective dose than Au nanoparticles.

Carbon Nanotubes

The 3 highest concentrations of SWCNT have statistically relevant effects in *Drosophila* embryo viability. Furthermore, treatment with SWCNT shows a shift in scoring criteria with highest mortality from late embryogenesis to L1, from the 4th to the 5th concentration. These results suggest that SWCNT presents a behavior similar to Au and TiO_2, were embryo mortality is delayed by a shift in scoring criteria with highest mortality from late embryogenesis to L1 and then shifts back. This could be confirmed by testing higher concentrations to see if mortality shifts from L1 to late embryogenesis or even immediately after injection.

On the other hand, MWCNT have statistically relevant effects in *Drosophila* embryo

viability only at the lowest (PEC) and the highest concentration. Contrary to the rest of the nanomaterials, treatment with MWCNT does not show a clear shift in scoring criteria with highest mortality. MWCNT only show a slight shift from late embryogenesis to immediately after injection, at the 2nd concentration, but at the 3rd concentration is reverted back to late embryogenesis. This could be confirmed by testing concentrations slightly smaller and slightly higher than the 2nd concentration (5.0E-04 μg/μL) to establish if there is a relevant mortality shifts from late embryogenesis to L1 and back to late embryogenesis. Overall mortality results of SWCNT and MWCNT are in accordance to what others researchers have found (Jia et al., 2005). SWCNT show higher toxicity than MWCNT.

CNT have a tendency to form agglomerates (Wick et al., 2007) and there is an ongoing debate on whether or not the degree of agglomeration is able to modify CNT toxicity (Wick et al., 2007; Lewinski, Colvin and Drezek, 2008). With the current methodology the specific toxic effects cannot be identified but they can be deduced. The toxic effect could be due to chemical interactions between the biological environment and the nanomaterial or as a result of a physical obstruction. It is possible that as the concentration in the microtransfered solution increases so does the size of the clusters. An increase in cluster size will diminish the possibilities for dispersion as well as the surface area to volume ratio of the nanomaterial. Big enough clusters can be encysted if dispersion is being halted and a decrease in surface are to volume ration can decrease free terminals for interactions with the biological environment. Either case can explain a decrease in mortality after an increase in concentration. Mortality can again increase but a paced rate once a saturation threshold has been surpassed because with an increase in concentration both the possibilities of agglomeration and the presence of free un-clustered nanotubes increase. This could not only explain the effects of CNT, but also the effects of Ag, Au, and TiO_2 nanoparticle treatment.

Effects of Predicted Environmental Concentrations

Since there is no data available on the PEC for Fe, we decided to conduct our trials with the lowest employed concentrations at a similar order of magnitude to that of the ones established for TiO_2, Ag, and CNT. None of the IO nanoparticles have statistically relevant effects in *Drosophila* embryo viability when treated at the lowest concentration, suggesting that if the environmental concentration were to be with similar order of magnitude to that of other

nanomaterials there would not be a statistically relevant mortality effect.

Only MWCNT treatment showed statistically relevant effects in *Drosophila* embryo viability when treated at PEC, suggesting a possible threshold of minimal toxic dosage (MTD). Thus, helping establish the maximum allowable concentrations (MAC) in the environment. In the case of MWCNT more rigorous guidelines should be established since the PEC led to a statistically significant mortality effect.

Passive-Transport Nanomaterial Assessment

The direct contact exposure interaction route presents the possibility of assessing a nanomaterial's capability to cross complex biological membranes in order to model environmental exposure or assessing a nanomaterial's capabilities as a nanocarrier. The equipment employed for ICP-MS analysis was not able to detect internalized metal traces. This does not mean that nanomaterials were not able to cross the chorion and vitelline membranes. For this reason, higher concentrations, longer exposure times, and using equipment with lower detection limits in the ppt ranges could help us obtain detectable measurements.

CHAPTER IX

CONCLUSIONS

The purpose of this research was to present *Drosophila melanogaster* as a suitable *in vivo* model for nanomaterial assessment. We developed a cost-effective product-specific nanomaterial assessment platform with two different interaction routes that model interactions relevant to biomedical applications and environmental exposure. The two exposure routes allow for overall mortality quantification, identification of specific stage of mortality, and quantification of internalized nanomaterials.

The current data on nanotoxicity is insufficient and little consensus has been reached. This systematic methodology is general enough that can be employed in the assessment of any kind of nanomaterial formation. Therefore, is amenable at any stage of R&D allowing for the simultaneous assessment of toxicity and possible biomedical applications. This assessment includes a novel and simple methodology for volume quantification that allows for dosage extrapolation. Our assay consists of a uniform assessment that allows for overall mortality quantification, which can be normalized against a control trial of the solution the nanomaterials were suspended in. The controls also account for the mortality caused by the mechanical damage of microdelivery, leading to results independent of human manipulation. Consequently, making these results reproducible. This high-resolution assessment not only allows for a general evaluation of embryonic viability, but also for the identification of specific stage of mortality. In turn, this can render information in terms of minimal toxic dose, acuteness of toxic effect, maximum allowable concentration in the environment, and stability of surface modification as a function of how delayed are the toxic effects elicit by the nanocore.

The toxicity assessment of iron oxide, silver, gold and titanium dioxide nanoparticles, single wall carbon nanotubes and multiwall carbon nanotubes yield important information that can uncover certain aspects of the tested nanomaterials. The results on mortality at predicted environmental concentrations can help establish future safety regulations in terms of maximum allowable concentrations (MAC) in the environment, particularly for MWCNT. The results yielded are expected to lead to improvements in the design of nanostructures and the establishment of standardized regulations for characterization, handling, and disposal of

nanomaterials. Furthermore, our assessment can be further developed to establish more specific molecular interactions linked to toxicity of specific tissues or organs. The obtained data on nanomaterial interactions with biological membranes is inconclusive. Therefore, higher concentrations, longer nanomaterial exposure times, and using equipment with lower detection limits in the ppt ranges could help us obtain detectable measurements.

Drosophila allows us to register morphological changes throughout development and as future work this methodology could be adapted to other stages of development. The nanomaterials could be traced across the life cycle in the surviving embryos specially if employing fluorescently tagged nanomaterials. Other tools like: transgenic flies with fluorescent markers against caspase-3; lactate dehydrogenase (LDH), to identify necrotic tissue; detection of intact lysosomes, and detection of reactive oxygen species, to assess stress response, can be integrated as mortality markers. This way more specific conclusions could be reached and specific organ and/or system toxic effects can be assessed (i.e. neurotoxicity). As a validated model for human diseases, *Drosophila* also presents the possibility of simultaneously assessing effects on viability and nanomaterial applications in the treatment or understanding of such human diseases. Finally, *Drosophila*'s cost-effectiveness, requiring nanomaterial amounts in the nanogram ranges, increases the possibility of this assessment being conducted as a high-throughput assay.

CHAPTER X

REFERENCES

Ahamed, M., Posgai, R., Gorey, T. J., Nielsen, M., Hussain, S. M., & Rowe, J. J. (2010). Silver nanoparticles induced heat shock protein 70, oxidative stress and apoptosis in *Drosophila melanogaster*. *Toxicol. App. Pharm.* 242, 263-269.

Allouni, Z. E., Cimpan, M. R., Hol, P. J., Skodvin, T., & Gjerdet, N. R. (2009). Agglomeration and sedimentation of TiO_2 nanoparticles in cell culture medium. Colloids Surf B Biointerfaces, 68 (1):83–87.

Asharani, P. V., Wu, Y. L., Gong, Z., & Valiyaveettil, S. (2008). Toxicity of silver nanoparticles in zebrafish models. *Nanotechnology.* 19(5), 255102.

Ashburner, M., Golic, K. G., & Hawley, R. S. (Eds.) (2004). *Drosophila A Laboratory Handbook*. Cold Spring Harbor, NY: Cold Spring Harbor Laboratory Press.

Barandeh, F., Nguyen, P. L., Kumar, R., Iacobucci, G. J., Kuznicki, M. L., Kosterman, A., Bergey, E. J., Prasad, P. N., & Gunawardena, S. (2012). Organically modified silica nanoparticles are biocompatible and can be targeted to neurons *in vivo*. *PLoS One*. 7(1), e29424.

Barrera, C., Herrera, A. P., Zayas, Y., & Rinaldi, C. (2009). Surface modification of monodisperse magnetic nanoparticles for biomedical applications. *J. Magn. Magn. Mater.* 321(10), 1397-1399.

Bernards, A., & Hariharan, I. K. (2001). Of flies and men - studying human disease in *Drosophila*. *Curr. Opin. Genet. Dev.* 11, 274–278.

Campos-Ortega, J. A., & Hartenstein, V. (1985). *The embryonic development of Drosophila melanogaster*. Verlag, Berlin: Springer.

Carrero-Martínez, F, & Chiba, A. (2009). Cell adhesion molecules at the *Drosophila* Neuromuscular Junction. In Umemori, H., Hortsch, M. (Ed.), *The sticky synapse*. (pp11-36). New York, NY: Springer New York.

Chiba A. (1999). Early development of *Drosophila* Neuromuscular junction: A model for studying neural networks in development. In Budnik, V., Sian Gramates, L. (Ed,), *Neuromuscular Junction in Drosophila.* (pp. 1-19). New york: Academic Press.

Chien, S., Reiter, L. T., Bier, E., & Gribskov, M. (2002). Homophila: Human disease gene cognates in *Drosophila*. *Nucleic Acids Research*. 30(1), 149-151. <www.superfly.ucsd.edy/homophila>

Das, T., & Cagan, R. (2010). *Drosophila* as a novel therapeutic discovery tool for thyroid cancer. *Thyroid,* 20(7), 689-695.

Dobson, J. (2008). Remote control of cellular behavior with magnetic nanoparticles. *Nature*. 3, 139-143.

Drexle, K. E. (2004). Nanotechnology: From Feynman to Funding. *Bulletin of Science, Technology & Society*, 24(1), 21-27.

DuBois, D. & DuBois, D. F. (1916). A formula to estimate the approximate surface area if height and weight be known. *Arch Int Med.* 17, 863-71.

Fako, V. E., & Furgeson, D. Y. (2009). Zebrafish as a correlative and predictive model for assessing biomaterial nanotoxicity. *Adv Drug Deliv Rev*. 61(6), 478-486.

Featherstone, D. E., Chen K., & Broadie, K. (2009) Harvesting and preparing *Drosophila* embryos for electrophysiological recording and other procedures. *J Vis Exp.* (27), 1347.

Fischer, H. C., & Chan, WC. (2007). Nanotoxicity: the growing need for in *vivo* study. *Current Op. Biotech.* 18(6), 565-571.

Folwell, J. L., Barton, C. H., & Shepherd, D. (2006). *J. Exp. Biol*. 209 (10), 1988-1995.

Gehan, E. A. & George, S. L. (1970). Estimation of human body surface area from height and weight. *Cancer Chemother Rep*. 54, 225-35.

Gilbert, L. I. (2008). *Drosophila* is an inclusive model for human diseases, growth and development. *Mol. Cell. Endocrinol.* 293(1-2), 25-31.

Granchi, D., Ciapetti, G., Savarino, L., Cavedagna, D., Donati, M. E., & Pizzoferrato, A. (1996). Assessment of metal extract toxicity on human lymphocytes cultured *in vitro*. *J Biomed Mater Res*. 31(2), 183-191.

Gupta, A. K., & Gupta, M. (2005). Synthesis and surface engineering of iron oxide nanoparticles for biomedical applications. *Biomaterials*. 26, 3995-4021.

Hamburg, M. A. (2012). FDA's Approach to Regulation of Products of Nanotechnology. *Science*. 336: 299-300.

Haycock, G. B., Schwartz, G. J. & Wisotsky, D. H. (1978). Geometric method for measuring body surface area: A height-weight formula validated in infants, children and adults. *J Pediatr* 1978, 93, 62-6.

Herrera A. P., Barrera C., & Rinaldi C. (2008a). Synthesis and functionalization of magnetite nanoparticles with aminopropylsilane and carboxymethyldextran. *J Mat Chem.* 18, 3650–365.

Herrera, A. P., Rodríguez, M., Torres-Lugo, M., & Rinaldi, C. (2008b). Multifunctional magnetite nanoparticles coated with fluorescent thermo-responsive polymeric shells. *J Mat Chem.* 18, 855–858.

Hillyer, J. F., & Albrecht, R. M. (2001). Gastrointestinal persorption and tissue distribution of differently sized colloidal gold nanoparticles. *J Pharm Sci*. 90(12), 1927-36.

Hirth, F. (2010). *Drosophila melanogaster* in the study of human neurodegeneration. *CNS Neurol Disord Drug Targets*. 9(4), 504-23.

Hoang, B., & Chiba, A. (2001). Single-cell analysis of *Drosophila* larval neuromuscular synapses. *Dev. Biol.* 229(1), 55-70.

Hohr, D., Steinfartz, Y., Schins, R. P., Knaapen, A. M., Martra, G., Fubini, B., & Borm, P. J. (2002). The surface area rather than the surface coating determines the acute inflammatory response after instillation of fine and ultrafine TiO2 in the rat. *Int J Hyg Environ Health*. 205(3), 239-244.

Hunter, P. (2008). The paradox of model organisms: The use of model organisms in research will continue despite their shortcoming *EMBo reports*. 9(8), 717-20.

Hussain, N., Jaitley, V., & Florence, A. T. (2001). Recent advances in the understanding of uptake of microparticulates across the gastrointestinal lymphatics. *Adv Drug Deliv Rev*. 50(1-2), 107-42.

Jain, T. K., Reddy, M. K., Morales, M. A., Leslie-Pelecky, D. L., & Labhasetwar, V. (2008). Biodistribution, clearance, and biocompatibility of iron oxide magnetic nanoparticles in rats. *Mol Pharm.* 5, 316-27.

Jia, G., Wang, H., & Tan, L. (2005). Cytotoxicity of carbon nanomaterials: single-wall nanotube, multi-wall nanotube, and fullerene. *Env Sci Technol*. 39(5), 1378-138.

Johnston, H. J., Hutchison, G., Christensen, F. M., Peters, S., Hankin, S., & Stone, V. (2010). A review of the *in vivo* and *in vitro* toxicity of silver and gold particulates: Particle attributes and biological mechanisms responsible for the observed toxicity *Critical Rev in* Toxicology. 40(4), 328–34.

Kawaguchi, T., Hanaichi, T., Hasegawa, M., & Maruno, S. (2001). Dextran-magnetite complex: conformation of dextran chains and stability of solution. *J Mater Sci Mater Med*. 12(2), 121-7.

Keshishian, H. (1996). The *Drosophila* neuromuscular junction: A model system for studying synaptic development and function. *Annu Rev. Neurosci.* 19, 545-75.

Kiehart, D. P., Crawford, J. M., & Montague, R. A. (2007).Collection, dechorionation, and preparation of *Drosophila* embryos for quantitative microinjection: *Drosophila* Protocols. Sullivan, W., Ashburner, M., Hawley, R. S. Eds. Cold Spring Harbor Protocols: New York.

Kimbrell, G. A. (2006). *Nanotechnology and nanomaterials in consumer products: regulatory challenges and necessary amendment.* The International Center for Technology Assessment. FDA public meeting on technology.

Klöpffer, W., Curran, M. A., Frankl, P., Heijungs, R., Köhler, & A. Olsen, S. I. (2007). Nanotechnology and Life Cycle Assessment. A systems approach to Nanotechnology and the environment: Synthesis of Results Obtained at a Workshop Washington, DC 2–3 October 2006 European Commission, DG Research, jointly with the Woodrow Wilson International Center for Scholars.

Kroll, A., Pillukat, M. H., Hahn D., & Schnekenburger, J. (2009). Current *in vitro* methods in nanoparticle risk assessment: limitations and challenges. *Eur J Pharm Biopharm.* 72(2), 370-7.

Lademann, J., Weigmann, H., Rickmeyer, C., Barthelmes, H., Schaefer, H., Mueller, G., & Sterry, W. (1999). Penetration of titanium dioxide microparticles in a sunscreen formulation into the horny layer and the follicular orifice. *Skin Pharmacol Appl Skin Physiol*. 12(5), 247-56.

Lewinski, N., Colvin, V., & Drezek, R. (2008). Cytotoxicity of Nanoparticles. *Small*. 4 (1) 26-49.

Liu, T., Li, L., Teng, X., Huang, X., Liu, H., Chen, D., Ren, J., He, J., & Tang, F. (2011). Single and repeated dose toxicity of mesoporous hollow silica nanoparticles in intravenously exposed mice. *Biomaterials.* 32(6), 1657-68.

Liu, X., Vinson, D., Abt, D., Hurt, R., & Rand, D. M. (2009). Differential toxicity of carbon nanomaterials in *Drosophila*: Larval dietary uptake is benign, but adult exposure causes locomotor impairment and mortality. *Environ. Sci. Technol.* 43, 6357–6363.

Lnenicka, G. A., & Keshishian, H. (2000). Identified motor terminals in *Drosophila* larvae show distinct differences in morphology and physiology. *J. Neurobiol*. 43(2), 186-197.

Lubick, N. (2008). Nanosilver toxicity: ions, nanoparticles—or both? *Environ Sci Technol*. 42(23), 8617.

Margaritis, L. H., Kafatos, F. C., & Petri, W. H. (1980). The eggshell of *Drosophila melanogaster*: Fine structure of the layers and regions of the wild-type eggshell. *J. Cell. Sci*. 43, 1-35.

Massart, R. (1981). Preparation of aqueous magnetic liquids in alkaline and acidic media. *IEEE Transactions on Magnetics.* 17, 1247-1248.

Medina, C., Santos-Martinez, M. J., Radomski, A., Corrigan, O. I., & Radomski, M. W. (2007). Nanoparticles: pharmacological and toxicological significance. *Br J Pharmacol*. (5), 552-8.

Mohan, N., Chen C.-S., Hsien, H.-H., Wu, Y.-C., & Chang, H.-C. (2010). *In vivo* imaging and toxicity assessments of fluorescent nanodiamonds in *Caenorhabditis elegans*. *Nano. lett.* 10(9), 3692-3699.

Monteiro-Riviere, N. A., Namanich, R., Inman, A., Wang, Y., & Riviere, J. (2005). Multi-walled carbon nanotube interactions with human epidermal keratinocytes. *Toxicol Lett*. 155, 377-384.

Mosteller, R. D. (1987). Simplified calculation of body-surface area. *N Engl J Med***.** 317, 1098.

Mueller, N. C., & Nowack, B. (2008).Exposure modeling of engineered nanoparticles in the environment. *Environ. Sci*. Technol. 42, 4447–4453.

NNCO-NSET-NEHI. (2009). Report of the national nanotechnology initiative workshop: Nanomaterials and human health- instrumentation, metrology, and analytical methods. Part III of IV. (National Nanotechnology Coordination Office, Arlington,VA). Available online: http://eprints.internano.org/1687/1/ehsnanoandhumanhealthandinstrumentation.pdf

Norwegian Pollution Control Authority. (2008). Environmental fate and ecotoxicity of engineered nanoparticles. Report no. TA 2304/2007. Eds.: E.J. Joner, T. Hartnik and C.E. Amundsen. Bioforsk, Ås. 64 pp.

NSTC/NSET. (2000). National Nanotechnology Initiative: The Initiative and its Implementation Plan, NSTC/NSET Report. National Science and Technology Council, Washington, DC. Available online: http://nano.gov/node/243

Office of Science and Technology Policy, Office of Management and Budget, & Office of the United States Trade Representative. (2011). Policy principles for the U.S. decision-making concerning regulation and oversight of applications of nanotechnology and nanomaterials. In: Memorandum for the heads of executive departments and Agencies. Executive Office of the President, Washington, DC: Holdren J. P., Sunstein C. R., Siddiqui I. A. Available online: http://www.whitehouse.gov/sites/default/files/omb/inforeg/for-agencies/nanotechnology-regulation-andoversight-principles.pdf

Orgad, S., Nelson, H., Segal, D., & Nelson, N. (1998). Metal ions suppress the abnormal taste behavior of the *Drosophila* mutant malvolio. *J. Exp. Biol*. 201, 115-120.

Ostiguy, C., Lapointe, G., Trottier, M., Ménard, L., Cloutier, Y., Boutin, M., Antoun, M., & Normand, C. (2006). Health effects of nanoparticles. In: Studies and Research Projects Report R-469. Montreál, IRSST. 55 pp.

Ostiguy, C., Roberge, B., Ménard L., & Endo, C.-A. (2009). Best Practices Guide to Synthetic Nanoparticle Risk Management. Studies and Research Projects / Report R-599. Montréal, IRSST. 67 pp.

Pantarotto, D, Briand, J. P., Prato, M., & Bianco, A. (2004). Translocation of bioactive peptides across cell membranes by carbon nanotubes. *Chem Comm.* 16-17.

Park, J., An, K., Hwang, Y., Park, J.-G., Noh, H.-J., Kim, J.-Y., Park, J.-H., Hwang N.-M., & Hyeon T. (2004). Ultra-large-scale syntheses of monodisperse nanocrystals. *Nat. Mater.* 3(12), 891-895.

Peer, D., Karp, J. M., Hong, S., Farokhzad, O. C., Margalit, R., Langer, R. (2007) Nanocarriers as an emerging platform for cancer therapy. *Nat. Nanotechnol.* 2, 751-760.

Pisanic, T. R. 2nd, Blackwell, J. D., Shubayev, V. I., Finones, R. R., & Jin, S. (2007). Nanotoxicity of iron oxide nanoparticle internalization in growing neurons. *Biomaterials*. 28, 2572-2581.

Pluskota, A., Horzowski, E., Bossinger, O., & von Mikecz, A. (2009). In *Caenorhabditis elegans* nanoparticle-bio-interactions become transparent: silica-nanoparticles induce reproductive senescence. *PLoS One*. 4(8), e6622.

Posgai, R., Cipolla-McCulloch, C. B., Murphy, K. R., Hussain, S. M., Rowe, J. J., & Nielsen, M. G. (2011). Differential toxicity of silver and titanium dioxide nanoparticles on *Drosophila melanogaster* development, reproductive effort, and viability: Size, coatings and antioxidants matter. *Chemosphere.* 85(1), 34-42.

Poulson, D. F. (1994). Histogenesis, organogenesis, and differentiation in the embryo of *Drosophila melanogaster meigen.* In: Demerec M. (Eds.) *Biology of Drosophila* (pp. 182-228). Cold Spring Harbor, NY: Coldspring Harbor Laboratory Press.

Powell, J. R. (1997). Progress and prospects in evolutionary biology: the *Drosophila* model. New York: Oxford University Press.

Reading B. D. & Freeman B. (2005). Simple Formula for the Surface Area of the Body and a Simple Model for Anthropometry. *Clinical Anat.* 18, 126-130.

Reiter, L. T., Potocki, L., Chien, S., Gribskov, M., & Bier, E. (2001). A systematic analysis of human disease-associated gene sequences in *Drosophila melanogaster*. *Genome Res*. 11(6), 1114–1125.

Rodrigues V. P., Cheah Y., Ray K., & Chia W. (1995). *malvolio*, the *Drosophila* homologue of mouse NRAMP-1 (Bcg), is expressed in macrophages and in the nervous system and is required for normal taste behaviour. *EMBO J*. 14 (13):3007- 3020.

Rogers, E., Hsieh, SF., Rao, N., Schmidt, D., Bello, D. (2008). A high throughput analytical approach to screen for oxidative stress potential exerted by nanomaterials in a biologically relevant matrix: human blood serum. Toxicol *In Vitro*. 22:1639–1647.

Schulz, J., Hohenberg, H., Pflucker, F., Gartner, E., Will, T., Pfeiffer, S., Wepf, R., Wendel, V., Gers-Barlag, H., & Wittern, K. P. (2002). Distribution of sunscreens on skin. *Adv Drug Deliv Rev*. 54(Suppl 1), S157-63.

Singh, N., Jenkins, G. J. S., Asadi, R., & Doak, S. (2010). Potential toxicity of superparamagnetic iron oxide nanoparticles (SPION). *Nano Rev*. 1, 5358.

Soenen, S. J., Rivera, Gil P., Montenegro, J.-M., Parak, W. J., De Smedt, S. C., & Braeckmans, K. (2011). Cellular toxicity of inorganic nanoparticles: Common aspects and guidelines for improved nanotoxicity evaluation", *NanoToday*. 6, 446-465.

Suh W. H., Suslick K. S., Stucky G. D., & Suh Y-.H. (2009). Nanotechnology, nanotoxicology, and neuroscience Review Article. *Progress in Neurobiology*, 87(3), 133-70.

Sung, J. H., Ji, J. H., Park, J. D., Yoon, J. U., Kim, D. S., Jeon, K. S., et al. (2009). Subchronic inhalation toxicity of silver nanoparticles. *Toxicol. Sci.* 108(2), 452-61.

Sutter, T. R. (1995). Molecular and cellular approaches to extrapolation for risk assessment. *Environ. Health Perspect.* 103 (1995), 386–389.

Thomson, J. N. (2004). *Drosophila* as a model organism. *Drosophila Serv*. 84, 119-131.

Tickoo, S., & Russell, S. (2002). *Drosophila melanogaster* as a model system for drug discovery and pathway screening. *Curr. Opin. Pharmacol.* 2(5), 555-560.

Tkachenko, A. G., Xie, H., Liu, Y., Coleman, D., Ryan, J., Glomm, W. R., Shipton, M.K., Franzen, S., Feldheim, D. L. (2004). Cellular trajectories of peptide-modified gold particle complexes: comparison of nuclear localization signals and peptide transduction domains. *Bioconjug Chem*. 15(3), 482-90.

U S Food and Drug Administration. (2005). Guidance for Industry. Estimating the Maximum Safe Starting Dose in Initial Clinical Trials for Therapeutics in Adult Healthy Volunteers. [accessed 2011 Aug 21]; Available from: www.fda.gov/downloads/Drugs/GuidanceComplianceRegulatoryInformation/Guidances/UCM078932.pdf

Usenko, C. Y., Harper, S. L., Tanguay, R. L. (2007). *In vivo* evaluation of carbon fullerene toxicity using embryonic zebrafish. *Carbon* 45(9), 1891-1898.

Vignais, P. V. Vignais, P. M. (2010). *Discovering Life, Manufacturing Life.* New York: Springer-Verlag.

Wick, P., Manser, P., Limbach, L. K., Dettlaff-Weglikowska, U., Krumeich F., Roth, S. (2007). The degree and kind of agglomeration affect carbon nanotube cytotoxicity. *Tox. Lett.* 168 (2), 121–131.

Wu, J., Liu, W., Xue, C., Zhou, S., Lan, F., Bi, L., Xu, H., Yang, Z., & Zeng, F.-D. (2009). Toxicity and penetration of TiO2 nanoparticles in hairless mice and porcine skin after subchronic dermal exposure *Toxicol. Lett.* 191(1), 1-8.

Yamamoto, H., Sano, T., Hasebe, S. (2001). Automatic microinjection system using stereoscopic microscope. *Intelligent Data Acquisition and Advanced Computing Systems: Technology and Applications, International Workshop.* 83-86.